*Review Paper*

# Accounting for training data error in machine learning applied to Earth observations

**Arthur Elmes*[1,2], Hamed Alemohammad[3], Ryan Avery[4], Kelly Caylor[4,5], J. Ronald Eastman[1], Lewis Fishgold[6], Mark A. Friedl[7], Meha Jain[8], Divyani Kohli[9], Juan Carlos Laso Bayas[10], Dalton Lunga[11], Jessica L. McCarty[12], Robert Gilmore Pontius Jr[1], Andrew B. Reinmann[13, 14], John Rogan[1], Lei Song[1], Hristiana Stoynova[13, 14], Su Ye[1], Zhuang-Fang Yi[15], Lyndon Estes*[1]** [1]

[1] Graduate School of Geography, Clark University, Worcester, MA 01610, USA; reastman@clarku.edu (J.R.E.); rpontius@clarku.edu (R.G.P.); jrogan@clarku.edu (J.R.); lsong@clarku.edu (L.S.); sye@clarku.edu (S.Y.); lestes@clarku.edu (L.E.)
[2] School for the Environment, University of Massachusetts Boston, Boston, MA 02125, USA; arthur.elmes@umb.edu
[3] Radiant Earth Foundation, San Francisco, CA, 94105, USA; hamed@radiant.earth
[4] Department of Geography, University of California, Santa Barbara, CA 93013, USA; ravery@ucsb.edu
[5] Bren School of Environmental Science and Management, University of California, Santa Barbara, CA 93013, USA; caylor@ucsb.edu
[6] Azavea, Inc., Philadelphia, PA 19123, USA; lfishgold@azavea.com
[7] Department of Earth and Environment, Boston University, Boston, MA 02215; friedl@bu.edu
[8] School for Environment and Sustainability, University of Michigan, 48109, USA; mehajain@umich.edu
[9] Faculty of Geo-Information Science & Earth Observation (ITC), University of Twente, 7514 AE Enschede, The Netherlands; d.kohli@utwente.nl
[10] Center for Earth Observation and Citizen Science, Ecosystems Services and Management Program, International Institute for Applied Systems Analysis (IIASA), Laxenburg, A-2361, Austria; lasobaya@iiasa.ac.at
[11] National Security Emerging Technologies, Oak Ridge National Laboratory, Oak Ridge, TN 37831, USA; lungadd@ornl.gov
[12] Department of Geography and Geospatial Analysis Center, Miami University, Oxford, OH 45056, USA; mccartjl@MiamiOH.edu
[13] Environmental Science Initiative, Advanced Science Research Center at the Graduate Center of the City University of New York (CUNY), New York, NY 10065, USA; Andrew.Reinmann@asrc.cuny.edu
[14] Department of Geography and Environmental Science, Hunter College, New York, NY 10065, USA; Hristiana.stoynova@gmail.com
[15] Development Seed, Washington, DC 20001, USA; nana@developmentseed.org

*Correspondence: arthur.elmes@umb.edu, Tel. 1-304-906-7946 (A.E.); lestes@clarku.edu, Tel. 1-202-431-0496 (L.E.)

*This paper is a non-peer-reviewed preprint submitted to EarthArXiv. It has been submitted to MDPI Remote Sensing for peer review.*

**Abstract:** Remote sensing, or Earth Observation (EO), is increasingly used to understand earth system dynamics and create continuous and categorical maps of biophysical properties and land cover, especially based on recent advances in machine learning (ML). ML models typically require large, spatially explicit training datasets to make accurate predictions. Training data (TD) are typically generated by digitizing polygons on high spatial resolution imagery, by collecting *in situ* data, or by using pre-existing datasets. TD are often assumed to accurately represent the truth, but in practice almost always have error, stemming from 1) sample design, and 2) sample collection errors. The latter is particularly relevant for image-interpreted TD, an increasingly commonly used method due to its practicality and the increasing training sample size requirements of modern ML

algorithms. TD errors can cause substantial errors in the maps created using ML algorithms, which may impact map use and interpretation. Despite these potential errors and their real-world consequences for map-based decisions, TD error is often not accounted for or reported in EO research. Here we review the current practices for collecting and handling TD. We identify the sources of TD error, and illustrate their impacts using several case studies representing different EO applications (infrastructure mapping, global surface flux estimates, and agricultural monitoring), and provide guidelines for minimizing and accounting for TD errors. To harmonize terminology, we distinguish TD from three other classes of data that should be used to create and assess ML models: training reference data, used to assess the quality of TD during data generation; validation data, used to iteratively improve models; and map reference data, used only for final accuracy assessment. We focus primarily on TD, but our advice is generally applicable to all four classes, and we ground our review in established best practices for map accuracy assessment literature, which are essential to follow for TD error accounting. EO researchers should start by determining the tolerable levels of map error and appropriate error metrics. Next, TD error should be minimized during sample design by choosing a representative spatio-temporal collection strategy, use of spatially and temporally relevant imagery and ancillary data sources during TD creation, and selection of a set of legend definitions supported by the data. Further, TD error can be minimized during the collection of individual samples by use of consensus-based collection strategies, by directly comparing interpreted training observations against expert-generated training reference data to derive TD error metrics, and by providing image interpreters with thorough application-specific training. We strongly advise that TD error is incorporated in model outputs, either directly in bias and variance estimates or, at a minimum, by documenting the sources and implications of error. TD should be fully documented and made available via an open TD repository, allowing others to replicate and assess its use. To guide researchers in this process, we propose three tiers of TD error accounting standards. Finally, we advise researchers to clearly communicate the magnitude and impacts of TD error on map outputs, with specific consideration given to the likely map audience.

**Keywords:** training data; machine learning; map accuracy; error propagation

## 1. Introduction

Recent technological advancements have led to a new era in Earth observation (EO, also known as remote sensing), marked by rapid gains in our ability to map and measure features on the Earth's surface such as land cover and land use (LCLU) [e.g. 1,2], vegetation cover and abundance [3], soil moisture [4], infrastructure [5,6], vegetation phenology [7–9], and land surface temperature [10,11]. The resulting data are used by an expanding set of disciplines to gain new insights into socioeconomic and environmental dynamics, such as community-level poverty rates [12], changes in surface water [13] and forest cover [14], and carbon accounting [15]. As such, EO is increasingly shaping our understanding of how the world works, and how it is changing.

These breakthroughs are facilitated by several technological advances, particularly the increasing availability of moderate (5-30 m), high (1-5m, High Resolution, HR), and Very High Resolution (<1 m, VHR) imagery, as well as new machine learning (ML) algorithms that frequently require large, high quality training datasets [16–21]. Large training datasets have been necessary for decades in the production of continental and global maps [1,2,22,23], and in the current data-rich era, the impact of TD quality and quantity on map accuracy is even more relevant, especially for maps generated by data-hungry ML algorithms [24–29]. Errors in these products in turn impact the veracity of any downstream products based on those maps [30]. While progress in algorithmic performance continues apace, standards regarding the collection and use of training data (TD) remain uncoordinated across researchers [31]. Additionally, much of the research and development of big data and ML is occurring in industry and the fields of computer science and (non-spatial) data science, leaving a potential knowledge gap for Earth Observation (EO) scientists [32,33].

The measurement and communication of map accuracy is a mature topic in EO and related fields, with a variety of metrics and approaches tailored to different data types, analyses, and user groups [34–42]. This includes substantial work to measure error in map reference data (i.e. the independent sample used to assess map accuracy) and account for its impact on map assessment [31,35,43,44]. However, focus on the quality and impacts of TD error has been less systematic. While several efforts have been made to use and evaluate the impact of different aspects of TD quality (noise, sample design, and size) on classifiers [27,29,45–50], much of this work focuses on exploring these issues for specific algorithms [28,45,50,51]. This previous research shows that the impact of TD error can be substantial but varied, suggesting that a more comprehensive approach to this issue is warranted. Furthermore, while TD and map reference data are often collected using the same approaches [52–54] and generally subject to the same errors, the existing procedures to minimize and account for map reference errors [31,35,43,44] are not necessarily relevant for quantifying the impacts of TD error. The problems associated with TD error can be summarized as follows:

1. The 'big data' era vastly increases the demand for TD
2. ML-generated map products rely heavily on human-generated TD, which in most cases contain error, particularly when developed through image interpretation
3. Uncertainty in TD is rarely assessed or reported, and TD are often assumed to have perfect accuracy [27] (which is also common with map reference data [54])
4. TD errors may propagate to downstream products in surprising and potentially harmful ways (e.g. leading to bad decisions) and can occur without the map producer and/or map user's knowledge. This problem is particularly relevant in the common case where TD and reference data are collected using the same methods, and/or in cases where map reference data error is not known or accounted for, which is still common [54]

These problems suggest a pressing need to review the issues surrounding TD quality and how it impacts ML-generated maps, and to recommend a set of best practices and standards for minimizing and accounting for those errors, which are the primary aims of this paper. Although map error can also originate from other sources, such as the specific ML classifier selected or the parameterization approach used [28,55,56], we focus solely on issues of input data quality. As such, this paper complements existing work focused on assessing final map accuracy [34–38,41,42].

This paper is organized into four sections. In section 1, we review current practices in the treatment of TD for categorical and continuous map creation. We also cover map accuracy procedures, given that the two processes are often intertwined and affected by many of the same issues [47], and accuracy assessment procedures are needed to assess the impacts of TD error. In section 2, identify the most common sources of TD error and inconsistency. In section 3, we illustrate the impacts of uncertainty in TD generation with case studies that span a range of typical EO applications, including building and road mapping, global surface flux estimates, and mapping agricultural systems. In section 4, we propose guidelines for i) best practice in collecting and using TD, including definition of acceptable accuracy levels, ii) minimizing TD errors associated with training sample design error and collection, iii) characterizing and incorporating TD error in final map outputs, and iv) communicating TD error in scientific and public documentation.

### *1.1 Current Trends in Training Data Collection*

A large proportion of remote sensing projects make some use of TD, typically created either using geolocated *in situ* data [43,57], by visually interpreting high and/or very high resolution spatial resolution imagery [23,58,59], or by interpreting the images to be classified/modeled themselves [e.g. 52,53,60,61]. Of these collection methods, image interpretation is increasingly common [62], particularly with the rise in crowdsourcing initiatives [19,63]. As such, mapping is strongly constrained by the creation of TD, which (much like map reference data) are often treated as absolute 'truth', if for no other reason than that their accuracy is assumed to be perfect [27,35,44,64]. However,

multiple sources of error are possible and indeed likely in TD, whether collected *in situ* or via image interpretation [57].

The use of large, data-intensive ML algorithms continues to grow in many fields, including remote sensing. Neural Networks (NN)s represent an increasingly used class of ML algorithms, with more complex NNs such as Convolutional Neural Networks (CNN) producing higher output accuracy [65]. While some forms of ML can function effectively with smaller training datasets, the quality of these data is nevertheless critically important [25,28,48]. Additionally, the increasingly popular large-scale, high-complexity NNs require substantially more TD than traditional statistical models, and like many ML approaches are sensitive to noisy and biased data, producing the logistical difficulty of creating very large, 'clean' training datasets [66–68].

Partially to address this need, several recent efforts have been devoted to producing extremely large training datasets that can be used across a wide range of mapping applications, and to serve as comprehensive benchmarks [69,70]. Similarly, a recent trend has emerged in large-scale mapping projects to employ large teams of TD interpreters, often within citizen science campaigns that rely on web-based data creation tools [19,71–73].

### *1.2 Characterizing Training Data Error*

Due to different disciplinary lineages, terminology associated with the various datasets used to train and evaluate map algorithms is sometimes contradictory or distinct. Here we harmonize terminology by defining four distinct types of data: training, validation, training reference, and map reference. ***Training data*** (TD) refers to a sample of observations, typically consisting of points or polygons, that relate image pixels and/or objects to semantic labels. ***Validation data*** are typically a random subset of TD that are withheld and used to fit ML model parameters and internally evaluate performance. ***Training reference data*** are expert-defined exemplar observations used to assess TD errors during or after data creation. ***Map reference data*** are independent observations used to assess final map accuracy; while these may be collected using many of the same procedures as the other three datasets [54], they have more stringent design protocols and can only be used to assess the final map product, rather than used iteratively in model or map improvement [54]. Map reference data are often referred to as the test set in ML literature [74], but we use the former term to align with the terminology commonly used by the EO community.

#### 1.2.1 Map Accuracy Assessment Procedures

Map accuracy assessment practices and standards are well-established in the EO literature [36,37,42,54,75]. We briefly review these procedures here because they are essential for quantifying how TD error impacts map accuracy. Additionally, the growing use of ML algorithms developed outside of EO has brought with it accuracy assessment practices and terminology that often differ nominally or substantively from those developed for EO [e.g., 76,77,78]. Reviewing EO accuracy assessment standards can therefore help to harmonize and improve accuracy assessment practices, while providing necessary context for procedures that can help to account for TD error.

The accuracy of a map is assessed by evaluating the agreement between the values of the mapped variables and those of a map reference variable, and summarizing those discrepancies using an accuracy metric [38,77]. A number of different accuracy metrics can be used, which vary depending on whether the variable of interest is categorical or continuous, with each type of variable having its own foundation for error analysis [79–83]. For categorical variables, this foundation is provided by the confusion matrix, in which rows (but sometimes columns) typically list how many mapped values fall within each category and columns (but sometimes rows) the distribution of map reference values for each category. In EO, the most widely used metrics calculated from the confusion matrix are user's accuracy (the complement of commission error), producer's accuracy (the complement of omission error), and overall accuracy (i.e. the complement of proportion error) [37]. A fuller explanation of accuracy metrics and other aspects of the error matrix can be found in existing publications [32,34,45,69,74–76]. Another widely used measure in EO is the Kappa Index of Agreement [77], but Kappa varies with class prevalence [78] and inappropriately corrects for chance

agreement [77], thus its continued use is strongly discouraged [37,77]. There are a number of other categorical accuracy metrics suitable for assessing the accuracy of a binary categorical variable, such as the F1 score [78], and the True Skill Statistic [84], which are described in the supplemental materials.

The scatter plot provides the basis for error analysis for continuous variables, wherein deviations between the mapped values plotted on the Y-axis are measured against those of the map reference on the X-axis. Several measures are used to summarize these deviations (see SI). The Root Mean Squared Error (RMSE, a.k.a. Root Mean Square Deviation, RMSD) and Mean Absolute Deviation (MAD) summarize deviations along the 1:1 line. The former has widespread use, but we recommend caution since it combines MAD with variation among the deviations [85–87]. Another widely used measure is the $R^2$, or coefficient of determination, but this measures deviation relative to the linear regression line, rather than the 1:1 line [80,85].

Beyond these, there are measures for comparing continuous mapped variables to a binary reference variable, including the Receiver Operating Characteristic (ROC) and the Total Operating Characteristic (TOC) [81,88,89]. The area under this curve (AUC) of an ROC/TOC plot is often used as a single measure of overall accuracy that summarizes numerous thresholds for the continuous variable [89]. There are also metrics for assessing the accuracy of object-based image analysis [OBIA, 90], which we do not cover here (but see the SI) because the choice of measure varies according to mapping objectives [62,91].

The creation of the map reference sample is an integral part of the accuracy assessment process and has two major aspects. The first of these is the design of the sample itself (i.e. the placement of sample units), which should be probability-based but can follow several different designs (e.g. simple random, stratified, cluster, systematic) depending on the application and *a priori* knowledge of the study area [77,92]. The second aspect is the response design, which governs the procedures for assigning values to the map reference samples [77,92]. These include the choice of the sample's spatial and temporal units, the source of the data that the sample extracts from (e.g. high resolution imagery), and the procedure for converting reference data values into map-relevant values [77,92]. For a categorical map in which the reference data source is high resolution imagery, the map reference sample is assigned labels corresponding to the map legend (e.g. a land cover scheme) based on a human supervisor's interpretation of the imagery [77,92].

A key aspect of response design is that map reference data should be substantially more accurate than the map being assessed, even though they are always likely to have some uncertainty [27,43,44,77,92]. This uncertainty should be measured and factored into the accuracy assessment [43,92]. However, in practice this accounting is rarely done, while map reference data uncertainty is also rarely examined [31,77,93]. This tendency is illustrated by Ye et al. [53], who reviewed 209 journal articles focused on object-based image analysis, finding that one third gave incomplete information about the sample design and size of their map reference data, let alone any mention of error within the sample. Errors in map reference data can bias the map accuracy assessment [42,90], as well as estimates derived from the confusion matrix, such as land cover class proportions and their standard errors [41]. To correct for such impacts to map accuracy assessment, one can use published accuracy assessment procedures, including variance estimators, that account for map reference error [35,43,44]. These approaches depend on quantifying errors in the map reference data.

### 1.2.2 Current approaches for assessing and accounting for training data error

Most of the aforementioned considerations regarding map reference data creation largely apply to TD, particularly since map reference data and TD may often be collected together [e.g. 52], provided the former are kept strictly separate to ensure their independence [77]. Considerations regarding TD may diverge with respect to sample design, as TD often needs to be collected in ways that deviate from probability-based sampling, in order to satisfy algorithm-specific requirements related to, for example, class balance and representativeness or the size of the training sample [28,48]. Another difference is that map TD can be usable even with substantial error [45,47,48]--although we show in Section 3 that TD error can propagate substantial map error--whereas map

reference data needs to have the highest possible accuracy and its uncertainty should be quantified, as described above [43,77,92].

If the quality of map reference data is often unexamined, TD quality may be even less so. To gain further insight into the level of attention TD receives in EO studies, we reviewed 30 recent, top-ranked[1] research papers describing land cover mapping studies (identified via keyword search on Google Scholar) [2,60,61,94–117]. This assessment showed that only 2 papers explicitly assessed the quality of the TD used in classification, while 16 made no mention of TD standards at all. Over 75% of these studies used image interpretation, as opposed to *in situ* data, in either training, accuracy assessment, or both. One-quarter of these papers used unsupervised classifiers in the processing chain to outline training areas, followed by image interpretation to assign labels to the polygons/pixels. Although only a snapshot, this finding suggests that key details regarding the design and collection of TD (and even map reference data) is lacking in the EO literature.

Even though TD quality appears to be largely unreported, efforts have been made to examine how TD error can impact ML-based classifications, typically within the context of evaluating specific algorithms. For example, research examining the effectiveness of Random Forests [118] for land cover classification also evaluated their sensitivity to TD error, sample size, and class imbalance [45,48,119], and similar work was done for Support Vector Machines [25,29,49]. Several studies comparing multiple ML algorithms also compared how each reacted variations in TD sample size and/or error [47,56,120,121]. Maxwell et al. [28] touch on a number of these TD quality issues in an even broader review of ML algorithms widely used in EO classification, but excluding newer deep learning approaches.

Beyond these examples, several studies have focused more explicitly on how to train ML-algorithms for remote sensing classification when TD error is present. Foody et al. [27] conducted tests to examine how two different types of TD labelling error impacted land cover classifications, with a primary interest in SVM. Similarly, Mellor et al.'s [45] study measured uncertainty introduced by TD error in a RandomForest classifier, with specific focus on class imbalance and labelling errors. Swan et al. [46] examined how increasing amounts of error introduced into the TD for a deep learning model impacted its accuracy in identifying building footprints. These studies collectively demonstrate that TD has substantial impact on ML-generated maps. They also reveal that there is no standard, widely accepted practice for assessing TD error, which, similar to map reference data, is generally not reported and thus implicitly treated as error-free [27].

## 2. Sources and Impacts of Training Data Error

In the following two sections we describe the common causes of TD error and explore its potential impacts. To describe causes, we divide the sources of TD error into two general classes: 1) errors stemming from the design of the training sample, which include many aspects of both sample and response design as described in existing literature on accuracy assessment (see 1.2.1 above), and 2) errors made when collecting the training sample, including the process of digitizing and labeling points or polygons when interpreting imagery, or collecting field measurements. In addressing the impacts of error, we provide a summary of potential problems, and then two concrete case examples for illustrative purposes.

### *2.1 Sources of Training Data Error*

#### 2.1.1 Design-related errors

With respect to TD sampling design, errors primarily relate to failures to adequately represent the spatio-temporal-spectral domains of the features of interest in the manner most suited to the specific ML algorithm being used [50]. This causes a disparity between the distribution of TD

[1]Based on the Google Scholar search algorithm results. Search performed January, 2019, with terms land cover and land use, including permutations of spelling and punctuation. Twenty-seven articles kept after initial screening for relevance.

compared to the true distribution of the mapped phenomenon in geographic and/or feature space [25–28]. This problem is highly relevant in ML approaches, which are sensitive to TD quality, including class balance, labelling accuracy, and class comprehensiveness relative to the study area's true composition [27].

Temporal unrepresentativeness is also a common source of error in the response design of TD, due to the prevalence of image interpretation as a source for TD. In this case, error arises when obsolete imagery is interpreted to collect training points or polygons and their associated labels [36,58]. The problem is illustrated in Figure 1, which contrasts smallholder fields that are clearly visible in a satellite base map (Bing Maps) with ground data collected in 2018. Center pivot fields were installed after the base map imagery was collected, but before ground data collection, creating a temporal mismatch between the base map and the *in situ* data. Labels generated from the base map would therefore introduce substantial error into an ML algorithm classifying more recent imagery. New HR satellites that have more frequent acquisitions [e.g. PlanetScope, 122] can help minimize such temporal gaps for projects that are designed to map present-day conditions (e.g. 2018 land cover), but cannot solve this problem for mapping projects covering earlier time periods (i.e. before 2016). The same can be said for aerial and Unmanned Aerial Vehicle acquisitions, which are typically limited in geographic and temporal extent [123]. While hardcopy historical maps can help supplement temporal data gaps, these data sources come with their own problems, such as errors introduced during scanning and co-registration, and unknown production standards and undocumented mapping uncertainties.

**Figure 1.** An example of potential training data error that can arise when image interpretation is conducted on older imagery. The underlying imagery is from Bing Maps, which shows smallholder agricultural fields near Kulpawn, Ghana. The white polygons were collected by a team of mappers (hired by Meridia) on the ground using handheld GPS in 2018. The smallholder fields were replaced by larger center-pivot irrigation fields sometime after the imagery in the base map was collected.

Spatial alignment can be a substantial source of response design-error when training with HR and VHR commercial satellite imagery. Due to their narrow swath widths, HR/VHR sensors are often tasked, resulting in substantially off-nadir image acquisitions [58]. Due to large view zenith angles and the lack of adequate digital elevation models, side overlapping imagery for stereo photogrammetry, or other relevant control points, HR/VHR imagery often does not meet the same orthorectification standards as coarser resolution, government operated satellites [124–126]. When integrating HR/VHR imagery acquired at different azimuth and elevation angles, features such as building roofs show offsets similar to those caused by topography. These offsets are particularly problematic for a) training repeated mappings of the same features, and/or b) when using an existing vector dataset such as OSM as TD [127–129].

TD collected by interpreting HR/VHR imagery is often co-registered with the coarser resolution imagery used as ML model data. This creates a potential spatial resolution conflict because the relationship between image objects and pixel size may be different, where objects delineated as spectrally homogenous areas in HR/VHR imagery may be part of mixed pixels in moderate or coarse resolution model imagery. This mis-match is similar to the concept of H-resolution versus L-resolution scene models proposed by Strahler et al. [130]; in H-resolution models, the objects of interest are substantially larger than the pixel size, and vice versa for L-resolution models. The incorporation of mixed pixels may degrade classification model performance, or at least introduce undesired spectral variability within classes [121,131,132]. This situation may be alleviated by displaying both HR/VHR imagery and/or other ancillary datasets as well as coarser model imagery during training data creation [133,134]. However, such practices may not be possible when training data are taken from previous research projects, or when they are to be applied in the context of time series analysis, in which spatial features change over time [e.g. 135].

Similar spatial resolution and scaling issues must be dealt with when combining *in situ* measurements with satellite observations for continuous variables. Field-collected data often cannot practically cover the entire area of a pixel in the model data, especially for moderate or coarse resolution imagery, and can thus induce scaling errors related to the modifiable areal unit problem [136,137]. Spatial representativeness assessments and interpolation methods are used to limit this problem for operational EO science products [138–141], but this issue is likely to be a source of error for most *in situ* TD samples.

Another design-related problem arises from large-scale data collection initiatives that are becoming increasingly common due to the expanding extent of modern EO analyses [e.g. 142]. These efforts, often conducted via crowdsourcing campaigns, typically enlist citizens to collect data a web-based platform [63,e.g. 143–145]. Examples include OpenStreetMap (OSM), Geo-Wiki [63], Collect Earth [146], DIYLandcover [144], and FotoQuest Go [147]. In cases where the resulting data might be purely voluntary [73], the resulting sample may lack spatial representativeness due to uneven geographic contributions [25,148].

### 2.1.2 Collection-related errors

There are several common forms of error that occur when collecting both TD and map reference data. The first of these are errors of interpretation [36], which are mistakes created in the process of manual image interpretation. Image interpretation is widely used to generate TD, and often does not yields inconsistent labels between interpreters [31,34,149,150]. Interpreters may lack experience in the task, or be unfamiliar with the context of the study area [e.g. 151]. In an unusually thorough analysis of error in image interpretation, Powell et al. [149] showed that inter-interpreter agreement was on average 86% but ranged from 46 to 92%, depending on land cover. This research, which relied on trained image interpreters, concluded that transitional land cover classes produce substantial interpretation uncertainty, which is particularly problematic since much land cover mapping effort is directed towards change detection. Another image interpretation study that used a crowdsourcing platform found that interpreters' average accuracy in digitizing crop field boundaries in high resolution imagery was ~80%, based on comparisons against training reference data [144]. This result held true whether the interpreters mapped several hundred sites or <50 (Figure 2), indicating that increased interpreter experience does not necessarily eliminate labelling error, even when analysts are highly seasoned [149]. These findings underscore the need to assess uncertainty in TD, as well as

map reference data, using predefined training reference data or inter-interpreter comparisons [43,57,149,152,153].

Labeling error may also result from inadequate or poorly communicated semantic class definitions [154,155], particularly when identifying land use, as opposed to land cover [156]. This is especially evident in urban environments, which not only exhibit high spatial and spectral heterogeneity, even within HR/VHR imagery [157], but are also are also semantically vague (i.e. hard to define) at the ground level. For example, Figure 3 shows a typical example of TD collection for mapping informal settlements (a.k.a slums), in Nairobi, Kenya, in which several trained interpreters separately delineate the same area [158]. Because slums may be defined by sociodemographic factors in addition to spatial and spectral properties, TD creation for such areas is prone to error stemming from semantic issues [155]. Complex classes such as slums may exhibit high variability between study areas, as local idiosyncrasies link the definition of slums to different physical, remotely observable characteristics. These characteristics make it hard to develop a generalizable mapping capability for informal settlements. These results further illustrate the importance of consensus mapping for image interpretation, particularly for heterogeneous target classes with vague or regionally idiosyncratic semantic definitions.

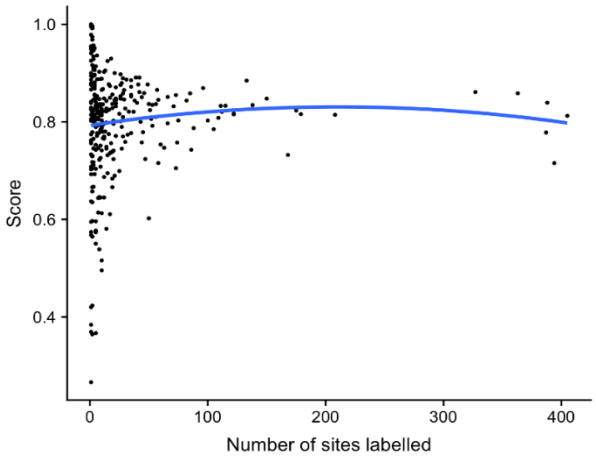


**Figure 2**: Number of sites mapped per worker versus the average score received at reference sites, where workers' maps were compared to reference maps using a built-in accuracy assessment protocol within a crowdsourcing platform for collect cropland data (Estes et al., 2016).

Categorical mapping projects typically define a crisp set of non-overlapping categories, rather than a fuzzy set [159,160]. However, many human and natural land covers exhibit continuous gradation between classes, implying that crisp map legends will necessarily cause semantic ambiguity for when image pixels in areas that are transitional between land cover types are labelled [161,162]. This problem is particularly acute with moderate and coarse resolution imagery [23]. When scene objects approximate the spatial dimension of the image resolution, local variance is highest, leading to poor classification accuracy [163]. While substantial research has been devoted to the issue of mixed pixels [83,131,132,164–166], crisp categories are still often relied on during the training and testing phases of image classification [167], although less crisp approaches based on fuzzy set theory are available [160,168]. Labelling errors can also arise if analysts are not properly trained on class definitions, or by poor data creation standards, such as failure to capture full metadata while in the field or during digitization, e.g. pertaining to difficult-to-determine cases or potential confusion

between spectrally, spatially, or conceptually similar classes [156]. Such inadequacies limit the analysis of TD error, and therefore the ability to account for error propagation.

Collection-related errors may be particularly acute in large-scale crowdsourcing campaigns or citizen science initiatives, which are increasingly valued for mapping projects due to their larger size and cheaper acquisition costs [19,63,144,145]. Such datasets are often collected rapidly and entail labeling many observations over a short period of time by participants who are not domain experts [147,169]. In such cases, label quality is a function of interpreter skill, experience, contextual

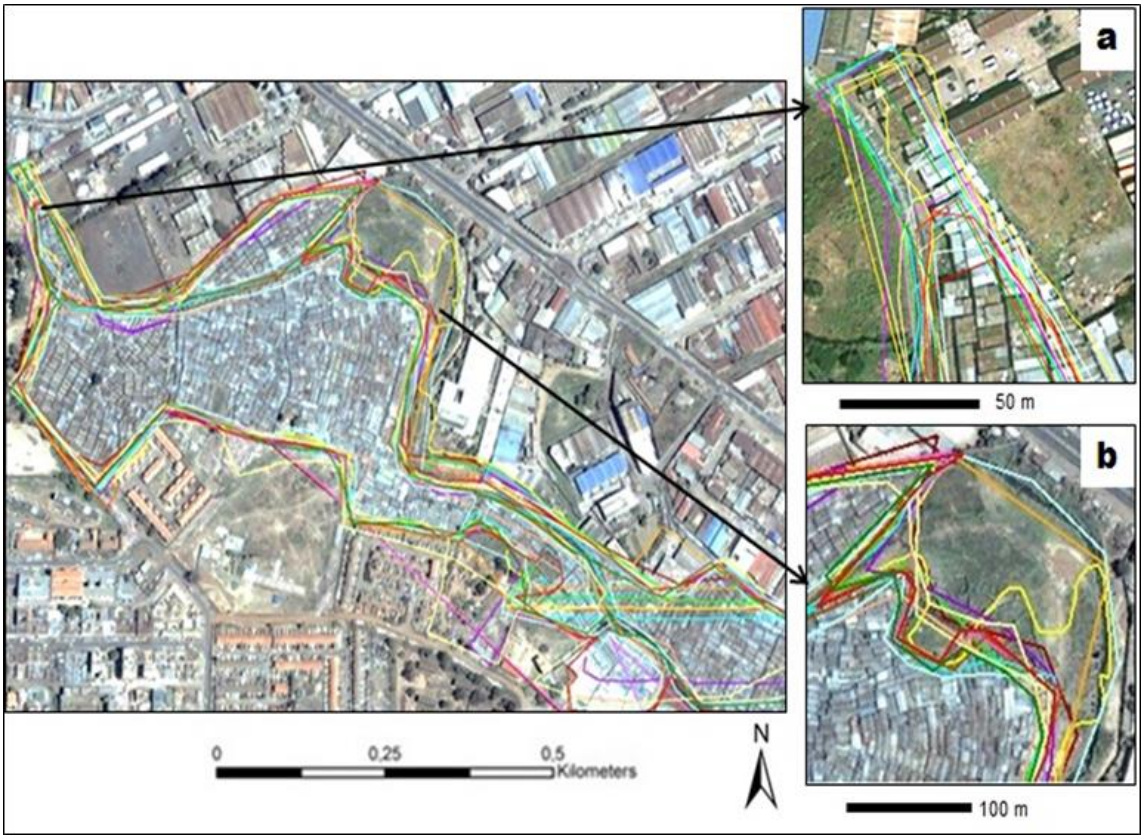


**Figure 3**: The challenges of mapping slum extent from image interpretation in Nairobi, Kenya. Each colored line indicates a different analyst's delineation of the same slum, illustrating semantic confusion. Adapted with permission from Kohli et al. (2016).

knowledge, personal interest, and motivation for involvement in the data collection [19]. Errors can be exacerbated if interpreters are inadequately trained or unfamiliar with the study area, or lack experience with EO data and methods. For example, delineation of different classes of urban land use may be extremely difficult without the benefit of local knowledge [155]. Furthermore, participants may be required to interpret HR/VHR satellite imagery collected over multiple sensors and dates and having varying quality (e.g. cloud cover percentage and atmospheric correction) and view/sun angles [170], which further complicates interpretation. Inadequate or confusing user interfaces may also lead to error [19,155]. Once crowdsourced/citizen science data have been post-processed for noise, they can be highly detailed and spatially extensive [63][66–68]. Nevertheless, quality problems in such datasets can be particularly hard to find and clean, and are thus an important source of TD error that may propagate through ML algorithms into map outputs [54,145,171]. Therefore, these data should be used more cautiously than expert-derived TD.

Errors also arise in *in situ* TD, caused by measurement error, geolocation inaccuracy, incorrect identification of relevant objects (e.g. vegetation species), and other such mistakes [172]. In addition to these factors, some feature types may also be difficult to discern on the ground [27]. Aside from these problems, there are many sources of technologically induced errors, such as defects in the

software or hardware of measurement devices, user input error, or calibration errors (e.g. in spectro-radiometers or other equipment). However, accounting for quantitative measurement error is more straightforward than thematic TD creation. Textbook tools to quantify measurement error are widely available, and *in situ* data collection procedures often include inter-analyst measurement comparison [173,174].

### *2.2 Impacts of Training Data Error*

TD errors carry through to impact the map production process and outcomes. From a design perspective, the size and class composition of TD is particularly impactful on ML algorithms, which are susceptible to overfitting and class imbalance problems [28,70]. Additionally, the assumption of representativeness of training pixels is often overstated, and many TD may in fact not be generalizable to broader scales (discussed by Tuia et al. [148]). TD errors arising from the collection process also impacts maps. Both design and collection-related errors may be particularly hard to discern, or quantify in absolute terms, if the error in the map reference data errors are unknown.

Several studies reviewed in Section 1.2.2 provide insight into how much TD error can impact ML-generated land cover maps, focusing on aspects of sample size and balance (design-related errors) and labelling error (collection-related error). This work shows that the impact of each error source varies according to the algorithm used. For example, support vector machines (SVMs) were relatively insensitive to changes in sample size, dropping by only 3-6% under TD size reductions of 85-94% [25,175]. RandomForests (RF) also proved robust to, but slightly more affected by, TD sample size, showing accuracy drops of ~4-10+% when TD was reduced by 70-99% [45,48,175]. Sample size also impacts the certainty of RF classification by lowering the mean margin (a measure of certainty related to the number of class votes) by ~50% for sample size reductions of 95% [45]. In contrast to SVM and RF, maps classified with single decision trees are highly affected by TD size, with 13% accuracy loss for TD reductions of 85% [25] all the way up 50-85% loss when TD size reductions of 50-70% [48,56]. Other models tested for TD sample size sensitivity include a neural network based on adaptive resonance theory, which had accuracy reductions of ~30 to ~65% when TD samples were halved [56], while a feed-forward neural network lost just 2% accuracy when TD was reduced by 85% [25].

Classifiers are also sensitive to class balance within the training data. For example, the accuracy of RF-generated maps declined by ~12 to ~23% and classification confidence fell ~25 to ~50% when TD class balances were highly skewed [45]. Notably, the ranges in these accuracy and confidence declines were attributable to differing TD sample sizes, showing the synergistic effect of sample size and class balance sensitivities. Maxwell et al. [28] provide a more comprehensive review of class imbalance for RF, SVM, artificial neural networks, and k-nearest neighbors (kNN), finding that all models were sensitive to class imbalance, but the impact was most felt in the accuracy for rare classes rather overall map accuracy.

The impact of TD labeling errors, also referred to as noise, vary substantially between mapping algorithms. SVMs and closely related derivatives appear least sensitive to mislabeling. SVMs lost just 0-5% in the accuracy or kappa of land cover classifications when 20-30% of TD samples were mislabeled either randomly or uniformly across classes [27,49,120]. Relative vector machines (RVMs) were even less sensitive under these conditions [2.5% accuracy loss for 20% mislabelling; 27], and an SVM designed specifically for handling noisy TD (context-sensitive semi-supervised SVM) was even more robust [2.4% reduction in kappa for 28% mislabelling; 49]. However, the impact of TD noise was greater for all three models when mislabeling was confined to specific classes. SVMs lost 9% accuracy and 31% kappa when 20-28% of samples in spectrally similar classes were mislabeled [27,49]. The RVM showed a 6% accuracy loss [27] and specialized SVM an 12% kappa reduction [49] under the same conditions. As with sample size, RF is the next least sensitive to TD noise [45,48]. Mislabeling 25% of TD samples reduced RF accuracy by 3-7% for a binary classifier and 7-10% for a multiclass model, with the ranges in accuracy loss also varying according to TD sample size [45]. Classification certainty was more heavily impacted by label error, dropping by 45-55%, as measured by the mean margin [45]. Other classification models showed larger impacts due to label noise,

including 11-41% kappa declines for a kNN [28% label noise; 49], and 24% [120,176] and 40-43% accuracy loss for a kernel perceptron and neural network, respectively, that were each trained with 30% of TD labelled incorrectly [56,120,176]. Single decision tree models were most sensitive to label error, registering 39 to nearly 70% accuracy declines for 30% label noise [56,120,176].

The aforementioned work provides substantial information on how TD error can impact the accuracy and certainty of older-generation ML classifiers. Further understanding of the consequences of these errors can be inferred from literature examining the impact of errors in map reference data. Map reference errors can substantially bias areal estimates of land cover classes, as well as the estimation of variance in those classes, particularly when examining land cover change [43,177,178]. While methods exist to incorporate map reference data error into map accuracy assessments and area estimates [35,43,44], and also to account for TD uncertainty in assessing classifier accuracy [45], there has been little work that shows how to address both TD and map reference error.

Less information is available regarding how TD error might propagate beyond the map it initially creates. Some insight can be found in a study that examined how error propagates from a primary land cover map into subsequent derived products [30]. This work used a high-quality reference cropland map to quantify the errors in 1 km cropland fractions derived from existing land cover datasets, and measured how these errors propagated in several map-based analyses that drew on cropland fractions for inputs. The results suggest that downstream errors were in some instances (e.g. carbon stock estimates, Figure 4) several fold larger than those in the input cropland maps, whereas in other cases (e.g. evapotranspiration estimates) errors were muted. In either case, the degree to which the error magnifies or reduces in subsequent maps is hard to anticipate, and the high likelihood that it could have the former effect means that any conclusions based on such land cover-derived maps must be treated with caution if the error propagation is not quantified. This analysis suggests how TD errors might impact the maps they generate and provides a potential method for quantifying their impacts on map accuracy.

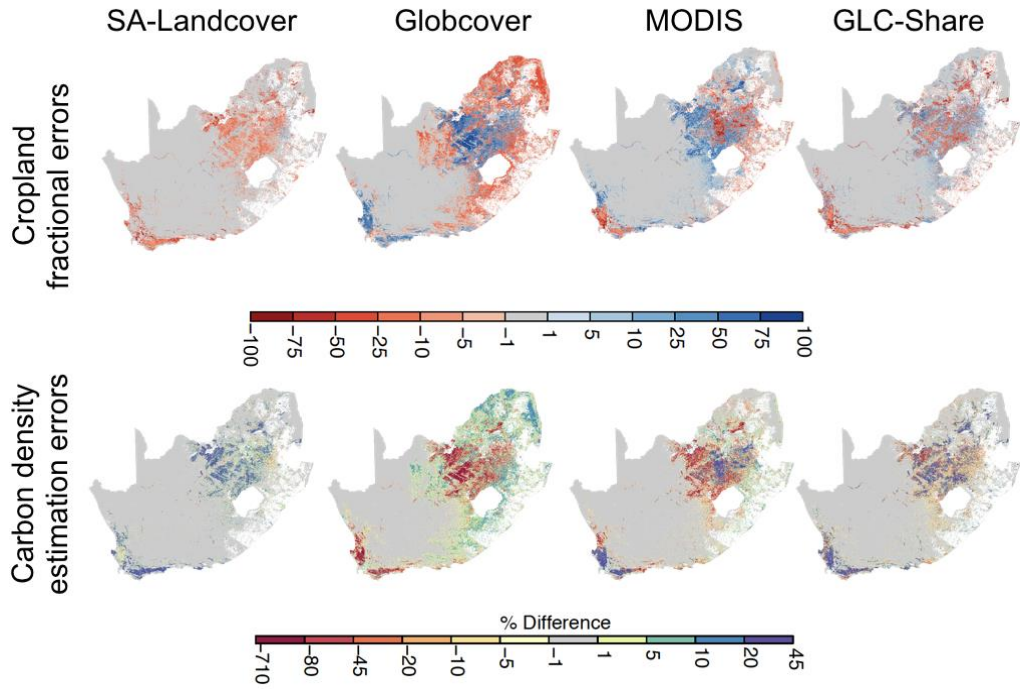


**Figure 4**: An examination of how error in pixel-wise cropland fractional estimates (expressed as a percentage, top row) can propagate error (expressed as a percentage) in maps that use land cover data as inputs, such as estimates of carbon density (bottom row). Figure adapted from Estes et al., (2018).

Another example illustrating the impact of map input errors is seen in the practice of using well-known standard datasets, such as the National Land Cover Map [NLCD, 179], to map quantities of interest, such as urban tree canopy biomass. Urban trees play a crucial role but in regional carbon cycles [180–182] but are often omitted from EO studies of carbon dynamics [e.g., MODIS NPP, 183]. As urban lands are expected to triple between 2000 and 2030 [184,185], the need to factor them into carbon accounting is pressing, but remotely mapping urban tree cover is limited by a) spatial resolutions that are too coarse for highly variable urban landscapes and b) TD that are often biased to forested, agricultural, and other rural landscapes. For these reasons, the Landsat-derived NLCD Percent Tree Cover (PTC) product [186], which estimates canopy cover at 30-m resolution across the U.S, provides a practical input for empirical models used to map tree biomass. However, previous studies showed uncertainty of this product in urban areas [186], and a tendency to underestimate urban canopy cover compared to a high resolution dataset. Therefore, to quantify the potential impact of NLCD PTC error on canopy biomass estimates, we compared the accuracy of the NLCD PTC dataset to canopy cover estimates derived from manually digitized VHR Imagery for a suburb of Washington, D.C., USA. We found that NLCD PTC underestimated canopy cover by 15.9%, particularly along forest edges (Figure 5) where it underestimated canopy cover by 27%. This discrepancy is particularly important in heterogeneous urban landscapes, where forest edges comprise a high proportion of total forest area. Scaling field data from forest plots to the entire study

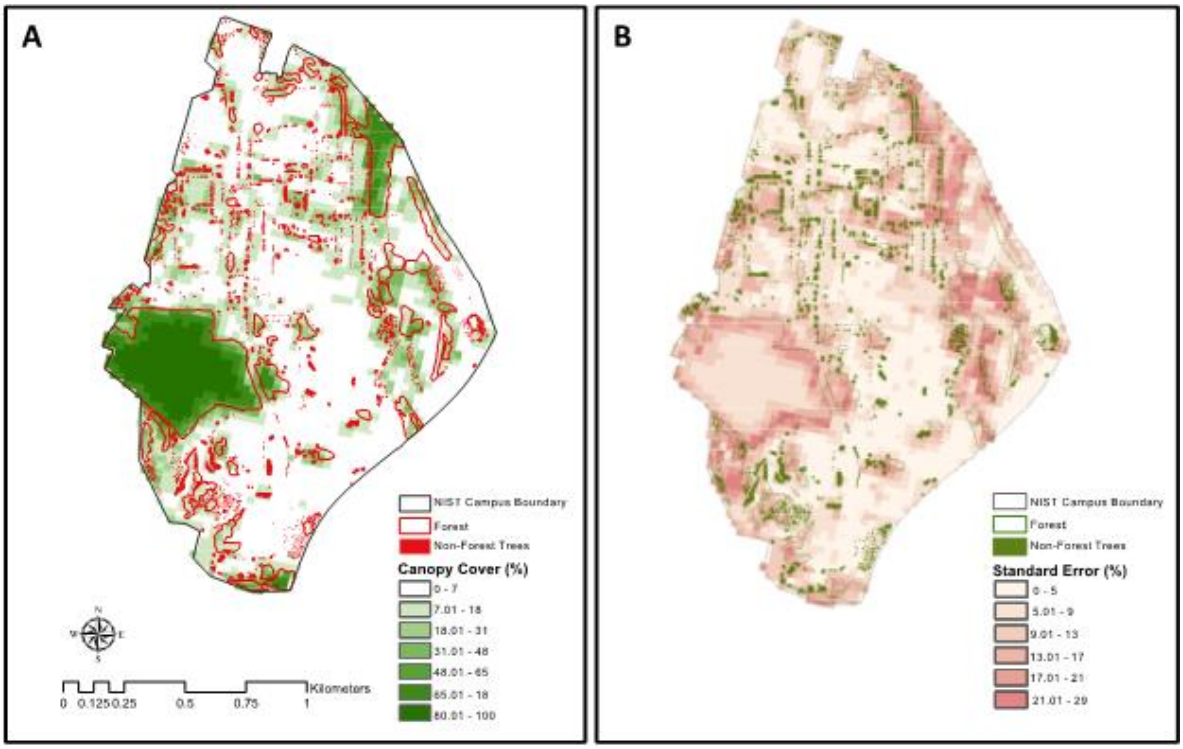


**Figure 5**: Spatial variations in canopy cover (A) and uncertainty in canopy cover estimates (B) in forested and non-forested areas of the heterogeneous suburban landscape of the National Institute of Standards and Technology campus in Gaithersburg, Maryland. Percent canopy cover at a 30-m resolution from the commonly used National Land Cover Database (NLCD) Percent Canopy Cover product (and its uncertainty) is superimposed over a high-resolution map of forested areas (hollow outlined polygons) and non-forest trees (e.g., street trees; solid polygons) that were manually mapped using <1-m resolution Wayback World Imagery. Note the lower estimates of percent canopy cover along forest edges (A) and the associated higher levels of uncertainty (B) using the NLCD product.

yielded an estimate of 8,164 Mg C stored in aboveground forest biomass, based on our manually digitized canopy cover map, compared to only 5,960 Mg C based on the NLCD PTC. This finding indicates the significance of these map errors for carbon accounting, as temperate forest carbon

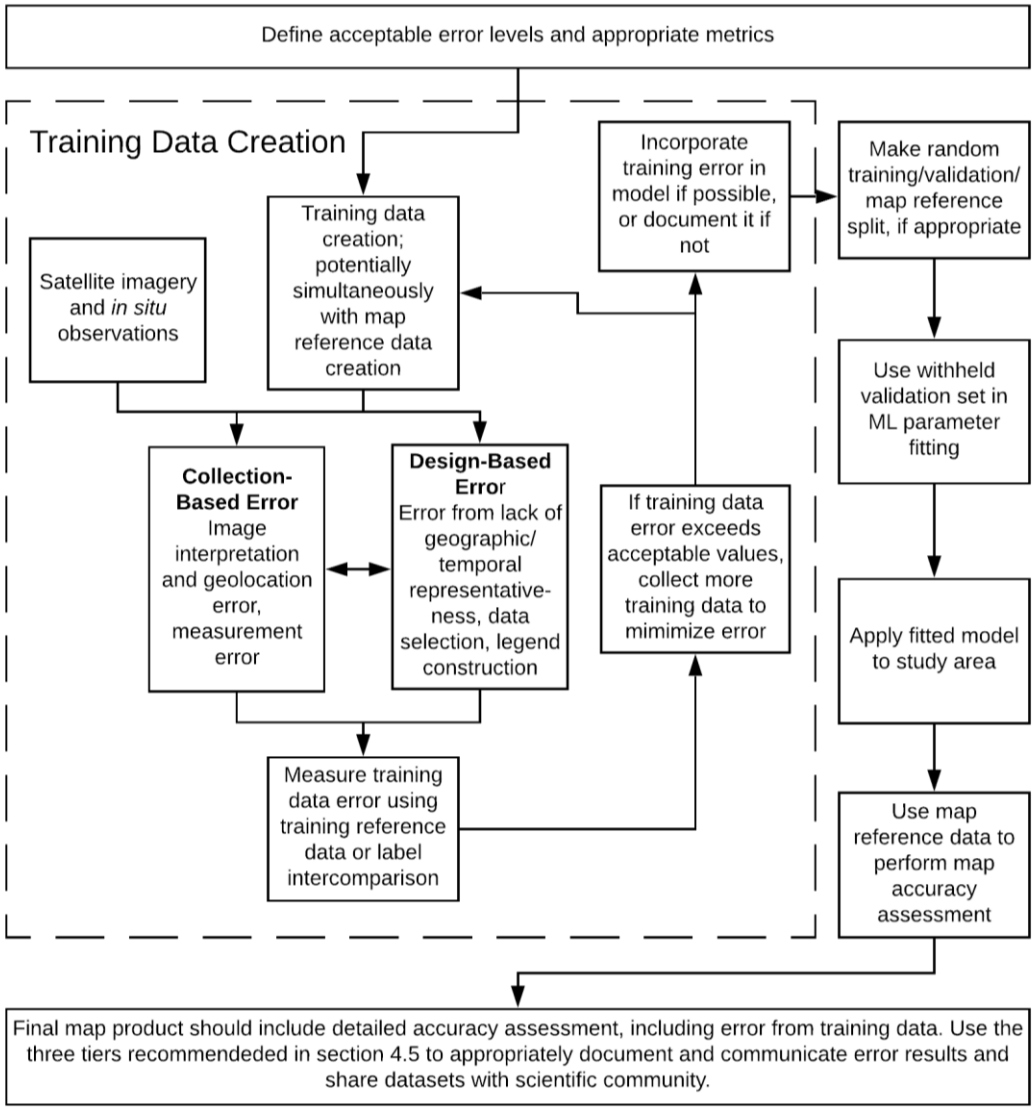


**Figure 6**: Flow chart of typical workflow for machine learning applications in Earth observation data.

storage and rates of sequestration are much larger (64% and 89%, respectively) than in forest interiors [187]. Quantifying errors in the NLCD is thus important for correcting subsequent estimates trained on these data.

These brief examples help illustrate the potential problems of TD error, but the range of potential impacts is as varied as the number of mapping projects underway across academic research, commercial operations, and the public sphere. To represent the growing set of remote sensing applications in which TD error may be encountered, we present a set of case studies below. To help lay a common framework, we show a typical methods sequence for a ML-based remote sensing analysis in Figure 6, which also helps clarify the terminology used in this paper. The figure shows the various sources and implications of error in the modeling and mapping process, beginning with issues in the data sources and sample design, and continuing through model training, validation, and ultimately in map accuracy assessment.

## 3. Case Studies

To better illustrate the potential impact of TD error, we provide several case studies across different mapping applications that represent the broad range of ML-based mapping and modeling applications that rely on TD.

## 3.1 Infrastructure Mapping

### 3.1.1 Incorporating Noisy Training Label Data

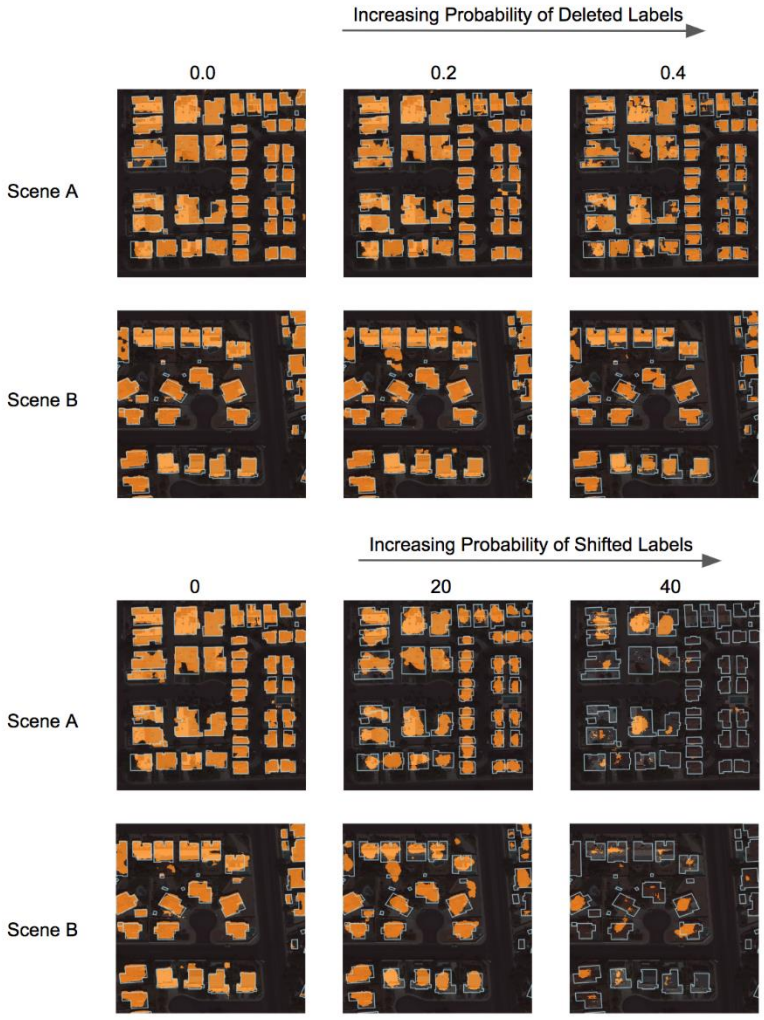


**Figure 7**: Predictions of the model trained on different noisy datasets. Each row shows a single scene over different noise levels. The top two rows show noisy drops, while the bottom two rows show noisy shifts. The ground truth is outlined in light blue, and the predictions are filled in orange.

Automated building footprint detection is an important but difficult mapping task, potentially benefiting a wide range of applications. The following case study illustrates the use of Raster Vision[2], an open source deep learning framework, to train several models for automated building detection from high resolution imagery[3]. These models perform best when trained on a large number of correctly labeled examples, usually generated by a paid team of professional labelers. An alternative, less costly approach was conducted in which a building segmentation model was trained using labels extracted from OpenStreetMap (OSM). However, the labeled training polygons generated from OSM contain errors: some buildings are missing, and others are poorly aligned with the imagery or missing details. This provides a good test case for experimentation on how noise in the labels affects the accuracy of the resulting model.

To measure the relationship between label noise and model accuracy, the amount of label noise was varied while holding all other variables constant. To do this, an off-the-shelf dataset (the SpaceNet Vegas buildings data set) was used in place of OSM, into which label errors were systematically introduced. To this relatively large training data set (~30,000 labeled buildings)[4], missing and imprecisely drawn building errors were systematically introduced, and the resulting model accuracy was measured. The experimental design consisted of two series of six datasets each, with random deletion or shift of buildings at increasing probabilities and magnitudes, respectively.

[2] https://rastervision.io/

[3] Additional detail available at: https://www.azavea.com/blog/2019/08/05/noisy-labels-deep-learning/

[4] https://spacenetchallenge.github.io/datasets/spacenetBuildings-V2summary.html

For each dataset, a UNet semantic segmentation model with a ResNet18 backbone was trained using the fastai/PyTorch plugin for Raster Vision[5]. These experiments, including data preparation and visualization, can be replicated using code at https://github.com/azavea/raster-vision-experiments/tree/master/noisy_buildings_semseg.

Figure 7 shows the ground truth and predictions for a variety of scenes and noise levels, showing that the quality of the predictions decreases with the noise level. Also, the background and central portions of buildings tend to be predicted correctly, whereas the outer periphery of buildings presents a greater challenge. These results are quantified in Figure 8, which shows F1, precision, and recall values for each of the noise levels below (see Table S1 for terminology description). The precision falls more slowly than recall (and even increases for noisy drops), which is consistent with the pattern of errors observed in the prediction plots. Pixels that are predicted as building tend to be in the central portion of buildings, leading to high precision.

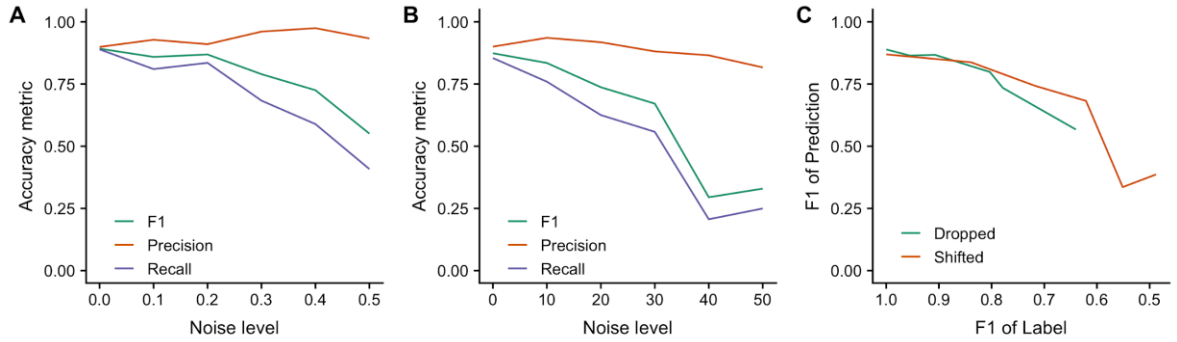


**Figure 8**: The precision, recall, and F1 scores across different noise levels are shown for the cases in which labels are randomly dropped (A) or randomly shifted (B).

In panels (A) and (B) of Figure 8, the x-axis shows the noise from randomly dropped and randomly shifted labels, respectively. Panel (C) combines the effects of noisy deletions and noisy shifts on accuracy in a single graph, showing F1 of the labels on the x-axis and F1 of the prediction on the y-axis. The F1 score of the noisy versus ground truth labels is a function of the pixel-wise errors; this metric has the benefit of measuring the effect of noise on error in a way that is comparable across datasets and object classes. For instance, a noisy shift of 10 in a dataset with large buildings might result in a different proportion of erroneous label pixels than in another dataset with small buildings. From this, panel (C) shows that while some of the shifted datasets have a greater level of noise, the prediction F1 scores are similar between the two series when the noise level is similar.

These experiments present a small step toward answering the question: how much accuracy is sacrificed by using TD from OSM? Preliminary results indicate, as expected, that accuracy decreases as noise increases and that the model becomes more conservative as the noise level increases, only predicting central portions of buildings. Furthermore, the noisy shift experiments suggest that the relationship between noise level and accuracy is nonlinear. Future work will quantify the functional form of this relationship, and how it varies with the size of the training set. Some preliminary work toward this goal has been described in Rolnick et al. [188], which focuses on image classification of Imagenet-style images.

One limitation of these results is that the magnitude of error in OSM for most areas is unknown, making it difficult to predict the effect of using OSM labels to train models in a generalized, global sense. "Noisy" error in OSM can be estimated by measuring the disparity between OSM labels to clean labels, such as the SpaceNet labels used in this case, providing a local estimate of OSM noise. A more general but less rigorous approach is to roughly estimate the noise level by visually inspecting the labels in OSM, and comparing to Figure 7, which shows examples of the labels at different noise levels.

[5] https://github.com/azavea/raster-vision-fastai-plugin

### 3.1.2 Detecting Roads from Satellite Imagery

Road networks constitute a critical geographical data layer used to assist national decision makers in resource allocation, infrastructure planning, vaccination campaigns, and disaster response, among others. However, accurate and up-to-date road networks are not available in many developing countries. High resolution satellite imagery, paired with deep learning methods, provides the capacity to detect and map roads at large spatial scales. This important goal, however, is dependent on availability of local high-quality TD.

To evaluate the impact of local TD availability on predicted road network accuracy, a study was carried out in Kumasi, Ghana [189]. Two datasets were used to train ML models: 1) the SpaceNet[6] dataset [190] in Khartoum, Sudan, and Las Vegas, USA, and 2) OSM data in Kumasi, Ghana. The SpaceNet Dataset includes high quality road labels with human expert validation, but unfortunately was not available in Kumasi, Ghana. Therefore, the latter study site relied on OSM data, consisting of crowdsourced labels with no accuracy assessment or expert validation. A series of experiments were carried out to assess the feasibility of using transfer learning, using the Raster Vision Python library for training and evaluation. For all MobileNet V2 models introduced in the following list, the

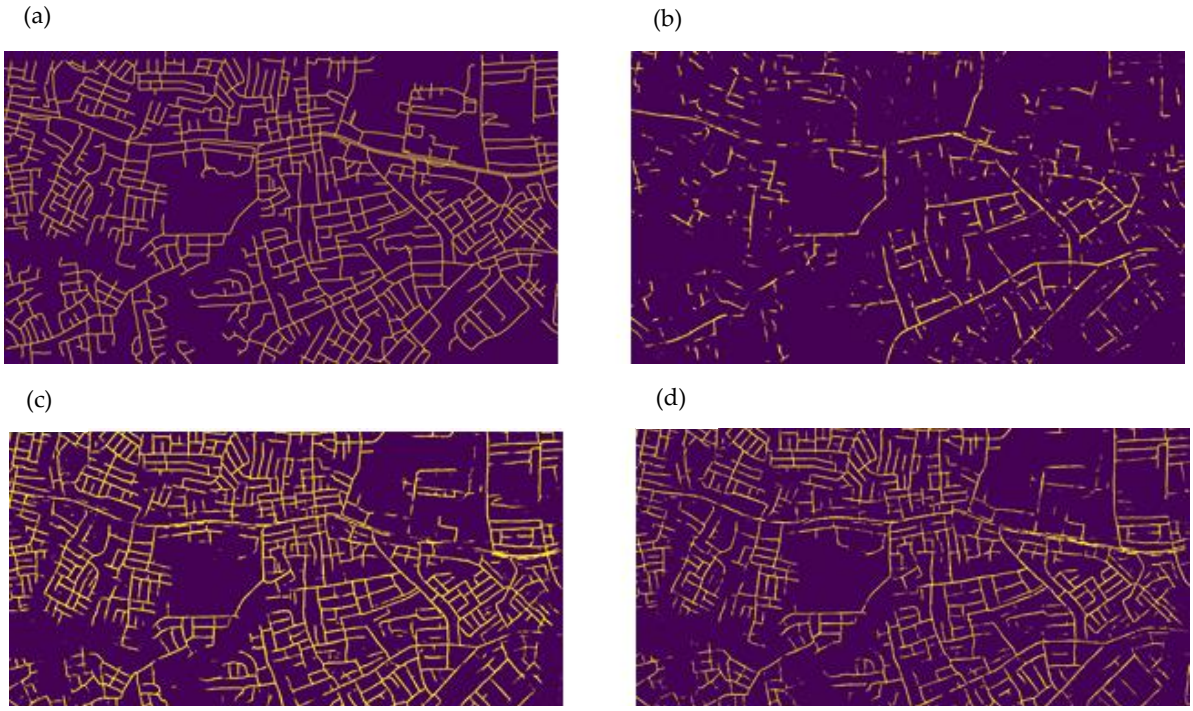


**Figure 9**: (a) Labels generated by experts for validation. (b) Predictions from the Khartoum Model. (c) Predictions from Kumasi Model. (d) Predictions from Khartoum Model retrained in Kumasi with 10K steps.

image chip size was set to 300 x 300 pixels, and the training/validation split was 80/20.

The Las Vegas Model was trained and validated on SpaceNet data in Las Vegas and produced very high accuracy predictions. However, when this model was used in Kumasi, it predicted very few roads, with only scattered road segments. The Khartoum Model was also trained using SpaceNet data in Khartoum. The Kumasi Model used Maxar WorldView-3 imagery and labels from OSM as input. OSM was used to test the quality of crowdsourced labels in training a road detection model. The Khartoum Model was then fine-tuned on OSM labels in Kumasi for three different steps of 100K, 50K and 10K. All models used the same hyperparameters, to isolate the role of TD on model performances.

[6] https://spacenetchallenge.github.io/

To validate the models' performance using an independent dataset, a set of expert labels were generated over a small part of Kumasi. Figure 9 shows the region with human expert data vetting, along with the three model predictions. The Las Vegas model is excluded from this figure as it does not have any meaningful prediction in Kumasi. Quantitative performance metrics were calculated using the human expert labels, which the models had been blind to during training. The results indicate that, as shown by Figure 9, the F1 score for roads was substantially higher for the Kumasi Model (0.6458) than when using the Khartoum model (0.3780). However, by retraining and fine-tuning the Khartoum model, the F1 score for roads increased to 0.6135. The full accuracy results for this experiment are presented in Table S2.

Based on these results, it is concluded that: 1) lack of diverse TD significantly limits the geographic applicability of models, as the types, surfaces, and arrangements of roads varies substantially between regions; 2) regional training datasets are essential for the model to learn the feature of roads in that region; and 3) transfer learning from a reasonably similar geography can help train models.

### *3.2 Global Surface Flux Estimates*

Fluxes at the land-atmosphere boundary play a key role in regulating water, carbon and energy cycles. These fluxes include latent heat flux (LE), sensible heat flux (H), and gross primary production (GPP). While these fluxes cannot be measured directly from remote sensing observations, other remotely sensed variables can be used to estimate these fluxes. Moreover, these three fluxes are highly coupled, and therefore a coupled model is ideal.

A fully connected neural network model was developed for this purpose [191], named Water, Energy, and Carbon with Artificial Neural Networks (WECANN). Inputs to WECANN are remotely sensed estimates of precipitation, soil moisture, net radiation, snow water equivalent, air temperature and solar induced fluorescence. The target variables for training the model were derived from outputs of global models. However, this presents the difficulty that the target variables are model outputs that can have substantial error, which will propagate in the WECANN model. To mitigate this problem, three independent estimates of each of the three fluxes (LE, H and GPP) were retrieved from the global models. Then a novel statistical approach, named Triple Collocation (TC, Figure S1, equation S1), was used to combine those estimates to a new dataset for training the WECANN model.

Triple collocation (TC) is a technique for estimating the unknown error (measured with standard deviations or RMSEs) of three mutually independent measurement systems, without treating any one system as zero-error "truth" [192]. The three measurement systems estimate a variable collocated in space and time, hence called Triple Collocation. Using these probabilities, at each pixel and at each time one of the three estimates of the target variable is randomly selected to generate the TD.

The results of WECANN model outputs were evaluated against ground measurements from global FLUXNET towers from 2007 to 2015 (Figure 10), using both the coefficient of determination and Root-Mean-Squared-Error (RMSE) to evaluate accuracy. These show that WECANN's correlation was on average 17% higher (range 8-51%) than that of any one of the three individual inputs, while the RMSE was 21% lower (range 4-54%). These differences provide a partial quantification of the error inherent in any one of these training inputs and show that by combining them using the TC technique, we can reduce error in an ML model for predicting the fluxes at global scale. This case study illustrates a means of assessing and accounting for error in training data for cases in which these data are not created specifically for the project, but rather are pre-existing data products with potentially quite different characteristics and potentially unknown error.

### *3.3 Agricultural monitoring*

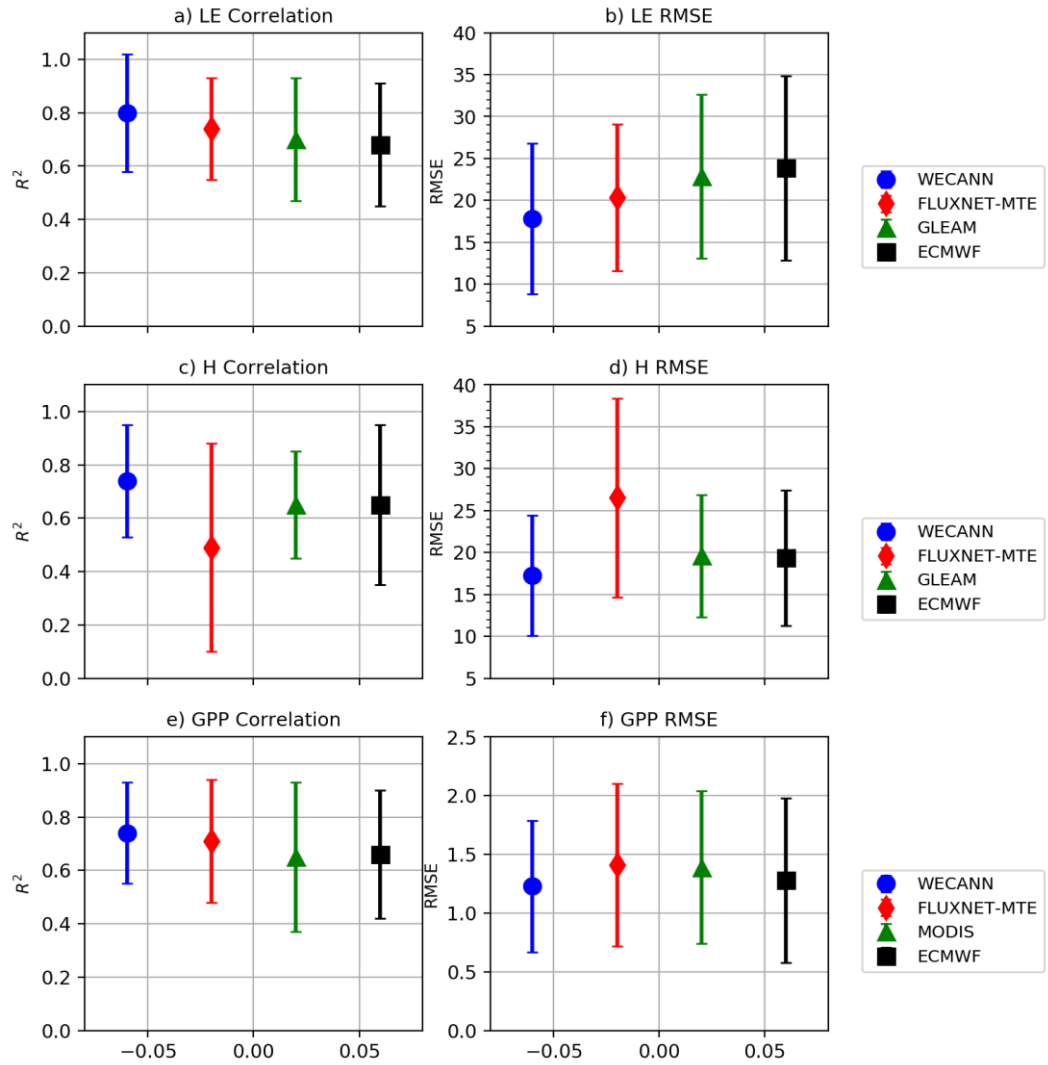


**Figure 10**: $R^2$ and RMSE of the WECANN model output against ground measurements from FLUXNET towers in comparison to the three datasets used to generate the target training data for LE (a, b), H (c, d) and GPP (e, f).

Two agricultural cases illustrate how TD error can impact both categorical and quantitative remotely sensed measures. The first relates to cropland mapping and is drawn from an ongoing study focused on mapping smallholder agricultural fields at high spatial resolution (3-4 m) in Ghana. The mapping method is based on "active learning", in which a RandomForest-based [118,193,194] ML algorithm is iteratively trained and validated by a crowdsourcing platform, which enlists human trainers to visually interpret and digitize field boundaries visible within the imagery (PlanetScope visual and near-infrared surface reflectance [122]) being classified [143,144,194]. The crowdsourcing platform incorporates a protocol for assessing the accuracy of training labels, in which each worker is periodically directed to a training reference site where the boundaries are already known but are not visible to the worker. Using these training reference sites, their maps are then scored using a multi-dimensional accuracy assessment algorithm [144], resulting in an average TD accuracy score for each worker that ranges between 0 (complete disagreement with reference) and 1 (perfect agreement). Each label site is mapped by at least five workers, and the resulting worker-specific accuracy scores are used within a Bayesian merging algorithm to combine the five sets of labels into a single consensus label, which is then used to train the RandomForest classifier. Here we use the worker-specific training accuracy scores to assess the impact of label quality on map accuracy, by assessing three variants of two RandomForest-generated maps, one over Central Ghana (~3,400 km$^2$) and one over Northern Ghana (~3,100 km$^2$). The first two maps were trained using labels generated

by the least accurate worker to map each training site, the second two by the most accurate worker to map each site, and the third using the consensus labels. The accuracy of each pair of maps was then assessed against the validation set (reserved consensus labels) using the True Skill Statistic [84] (sensitivity + specificity - 1, with scores ranging from -1 to 1). The results show a substantial difference in accuracy between the maps trained with the least and most accurate workers' labels (Figure 11A), with the former having 7-9% more skill than the latter, while maps based on consensus labels have ~3% more skill than those of the most accurate workers' labels.

The second case relates to remotely sensed crop estimates of wheat yields collected in 48 smallholder fields in Bihar, India in 2016-17 [195]. Yield data were collected via eight 2x1 $m^2$ crop cuts within each field, and PlanetScope-derived green chlorophyll vegetation indices (GCVI) were calculated over each field from imagery collected over four dates during the growing season (January 13, February 25, March 12, and April 14, 2017). A RandomForest regression was trained on the yield measured for each field, using the four dates of GCVI values as predictors. To test the effect of TD error on the resulting yield predictions, three types of noise were artificially introduced into the yield data used for training: 1) a systematic 0.5 ton/ha overestimate, and randomly distributed errors sampled from a normal distribution with a mean of 0 ton/ha and 2) standard deviations of 0.5 ton/ha

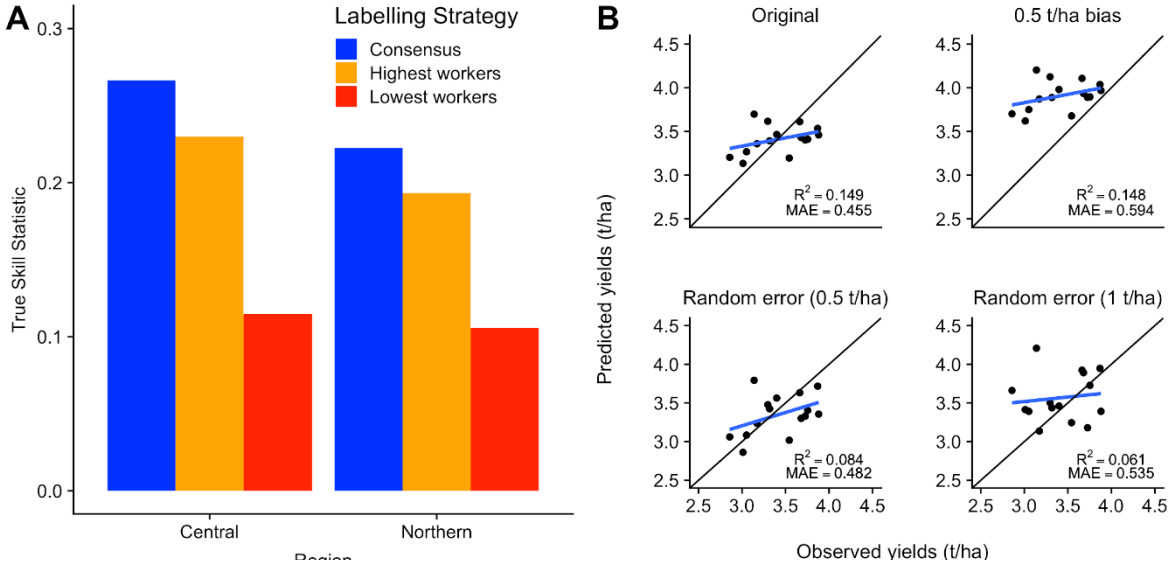


**Figure 11**. A comparison (A) of the accuracy (based on the True Skill Statistic) of cropland maps over two areas of Ghana when generated by labels of different levels of quality (red = least accurate workers' labels; orange = most accurate workers' labels; blue = "consensus" labels made by merging all workers' labels). (B) Results from a RandomForest model of wheat yields trained on satellite-derived vegetation indices, showing the relationship between predicted yield and independent observed yields, in terms of the fit against the 1:1 line and the regression slope of the relationship (points and regression line represent the mean of a single randomly selected model permutation). The average mean absolute error (MAE) and average regression $R^2$s calculated across all permutations are shown for each model.

and 3) 1 ton/ha. A baseline model fit to unperturbed data was also developed. Each model was trained on three separate randomly selected subsets of 32 perturbed observations, and the predictions were made for the remaining 16 held-out (independent) yield observations, which were not perturbed. This three-fold cross validation process was repeated 50 times, with each permutation using a different random seed to construct the folds, in order to achieve stable error metrics. The model performance was assessed by calculating the averages of the mean absolute error (MAE) of the prediction, and the $R^2$ of regressions fit between prediction and observed values (Figure 11B).

The results show that four models, including the baseline, compressed the range of yields, as seen in the shallow slope between observed versus predicted values, but prediction error was 18-31% higher when training yields had either the high level of random or systematic error within them. The

744 smaller amount of random noise only added about 6% error to the predictions, suggesting that
745 RandomForest is tolerant to some training error. Note that the average $R^2$ of the observed-predicted
746 regression fit was nearly the same for the systematic error case as the baseline, which shows that this
747 metric can be an unreliable measure of performance for quantitative measures, and that it is
748 important to assess fit against the 1:1 line and using a metric such as mean absolute error.

749 **4. Guidelines and Recommendations**

750 Our review and case studies show that the impacts of TD error on EO applications can vary, as
751 well as the procedures for assessing those impacts, but several best practices and guidelines can be
752 discerned within this work. Below we synthesize a set of suggested steps for minimizing and
753 accounting for TD error, within the context of undertaking and assessing the accuracy of a typical
754 ML-based mapping project.

755 *4.1. Step 1: Define acceptable level of accuracy and choose appropriate metric*

756 As a starting point, mapmakers should determine the minimum level of accuracy needed for
757 their application, using the accuracy metric(s) most appropriate for answering their questions [196].
758 For example, if the goal for creating a categorical map is to obtain an unbiased area estimate for a
759 particular land cover, it is essential to account for the map's commission and omission errors by
760 adjusting the proportional area estimate of the cover type derived from the map by the proportion of
761 that type estimated from the map reference sample [37,77,92]. For a continuous variable in which the
762 absolute accuracy of the mapped variable is most important, then the mean absolute deviation from
763 the 1:1 line is more informative than $R^2$ [86,87].
764 Error in the map reference data should also be factored in the selected accuracy metrics and the
765 resulting map-derived measures. Several published methods exist for categorical data (see Section
766 1.2.1). For continuous variables, the fit between the mapped and map reference variables can be
767 assessed using Type 2 regression, which allows for error in the dependent (map reference) variable
768 [197], unlike the more commonly used Type 1 regression. Determining map reference data error is
769 critical to determining overall map accuracy. The error in these data effectively determines the upper
770 limit of achievable map accuracy, as it is difficult (but not impossible; see [44]) to know whether a
771 model's predictions are more accurate than its map reference data; if the map reference data are only
772 90% accurate, then the map can be at most 90% accurate. Acceptable accuracy should thus be
773 determined relative to the accuracy of the map reference data, rather than the implicit assumption of
774 100%, which is widely used since map reference data are usually considered perfect [35,36,44,54,64].
775 Although the aforementioned steps relate primarily to concerns about map accuracy assessment,
776 they are essential to establishing best practices for map training. For one, without undertaking
777 rigorous accuracy assessment as described above, it is not possible to fully assess how TD error
778 impacts map accuracy. Secondly, the processes of map reference data and TD generation are often
779 tightly intertwined and impacted by many of the same sources of error (see Sections 1.2.1-2). The
780 procedures for minimizing and measuring errors in both datasets are thus often the same. Our
781 subsequent recommendations therefore cover both training and map reference datasets, except
782 where we indicate necessary distinctions.

783 *4.2. Step 2: Minimize design-related errors*

784 The next logical step in a mapping project is to design strategies for independently collecting the
785 training and map reference samples. Although there are numerous factors to consider, there are
786 several general aspects of design that can help minimize potential TD errors.

787 4.2.1 Sample design

788 The first of these relates to sampling design itself, meaning where, when, how many, and what
789 type of samples are placed (e.g. simple random, clustered, stratified, systematic). With respect to the
790 TD, to a certain extent this depends on the requirements of the selected ML algorithm, which can, for

example, have differing requirements with respect to geographic dispersal [50] and class balance [e.g. 28,45,78]. Geographic representativeness and the degree to which they capture the variability in the feature of interest is an important TD sample design consideration [50,58,144,198]. The road mapping case study shows the errors that can result when maps are trained with samples that do not adequately represent the features in a particular region. TD can in practice be highly localized or relevant for a limited spatial extent or temporal period [155,189]. This problem may become more relevant given the increase in stock or benchmark training libraries, and attempts to transfer pre-trained models to other regions, time periods, or scales of observation [70,199]. While such training libraries can be of immense benefit to large extent EO research, if these are to be relied on for training, their representativeness of the features of interest should be assessed, and augmented as needed, as in the Khartoum model case study (Figure 9D). For some widely used ML algorithms, such as RandomForests, the best practice appears to be to train with data collected within the mapping region [e.g. within a particular agroecoregion, 52,200], and to avoid over-generalizing or transferring models to other regions [201]. However, until more published studies are available, it is not clear whether this rule applies to deep learning models. When using citizen science or crowdsourcing approaches to generate these data, representativeness is ensured by directing labellers to the selected TD sites [e.g. 144], rather than having them select regions to map.

Samples should also be temporally representative of the imagery that is being classified [58]. That is, relative to the imagery being classified, the TD (and map reference) sample should be collected within a window of time that matches the characteristic rate of change of the feature being mapped. This interval can be estimated by measuring the temporal autocorrelation in the feature of interest [202]. For rapidly changing phenomena, such as deforestation events, snow/ice melt, and vegetation coverage during phenological transition, the sample may need to be captured within a few days or weeks of the acquisition of the imagery being classified, whereas for slower-moving features a sample collected within a few years may be sufficient.

In cases where training and reference samples are generated simultaneously, it is essential that TD sample design not undermine the standards required for an independent, probabilistic map reference sample [*sensu* 64]. Stehman and Foody [54] describe procedures for ensuring the independence of the map reference sample in such cases. Beyond those considerations, it is important to note that the map reference sample's independence is compromised when it is used to iteratively refine the mapping algorithm. This problem can best be understood within the context of cross validation, which is appropriate for ML parameter tuning [e.g. 28]. However, when the number of folds exceed one (as in our yield estimation case study; Figure 11B) then the portions excluded from training lose statistical independence and can no longer serve as the map reference [74]. Map reference data independence may also be undermined when training sites are selected iteratively, in order to increase their representativeness and improve ML performance [52,e.g. 143]. If the gain due to new training sites is assessed against the map reference, then it will also lose independence after the first iteration. Moreover, any error in the map reference sample will be integrated into the final map. Xiong et al. [52] avoided this problem by visually assessing whether their classifier improved map quality after having new TD points added to the initial sample. A more quantitative approach is to divide an initial sample into three splits: one for training, the second for validating algorithm improvements, including those related to the addition of new training sites, and the third as the map reference, used only for final accuracy assessment. This partitioning approach can be implemented in the mapping platform used in the cropland mapping case study [Figure 11A, 193].

#### 4.2.2 Training Data Sources

The requirements for temporal representativeness make the source of training imagery a critical consideration for projects that rely on image interpretation. The use of basemap imagery is not recommended for training maps of dynamic features, given their broad range and uneven distribution of image ages [58], unless the age of the imagery being classified can be matched to that of the training imagery. Otherwise, there is substantial potential for introducing error into the mapping algorithm (e.g. Figure 1), and its impact may be hard to assess, particularly if the map

reference sample is collected from the basemap. The goal of temporal representativeness must be balanced with the need to have a sufficiently high spatial resolution for accurate image interpretation, which helps minimize errors during the collection of the sample (see Step 3). Beyond matters of cost, this tradeoff is one reason why HR/VHR basemaps are widely used [58]. New commercial imagery, such as PlanetScope [122], which are collected at high temporal frequency (near-daily) with a spatial resolution sufficient for many visual interpretation tasks (3-4 m), may be a preferable source of training imagery for developing maps representing the post-2016 period. Finally, in designing an image-based sample, it is also important to consider additional characteristics that can influence interpreters' judgement, such as atmospheric quality (e.g. clouds, haze), sensor view angle, sun angle, spectral band selection, and image contrast stretches [71].

#### 4.2.3 Legend design

For thematic maps, legend design merits special consideration as it relates to TD, particularly for multi-temporal and/or large area projects that rely on multiple image datasets [58]. As discussed in section 2 above, objects of interest, including land cover types, should be at least twice as large as the pixel resolution of the imagery used in the classification algorithm, assuming a requirement for spectrally pure pixels [130,163,203]. When image spatial resolution is too coarse relative to the scene elements of interest, image interpretation errors are likely due to mixed pixels [121,131,132]. This implies that in designing a legend, researchers should select classes that can be mapped effectively using the coarsest resolution imagery that will be incorporated in the model, and avoid the problem of collecting training samples with mixed pixels [e.g. 52]. This consideration is particularly relevant since HR/VHR imagery is often used to create TD and map reference data, while the mapping algorithm is applied to moderate or coarse resolution imagery [e.g. 52,114,204,205]. Alternatively, researchers may opt to select a classification workflow which explicitly incorporates mixed pixels [91,160,e.g. 168].

Continuous TD, particularly those collected *in situ*, are often point samples, and therefore a sampling protocol should be used to match field measurements and pixel dimensions in order to avoid scaling problems associated with the modifiable areal unit problem [136,137]. Spatial representativeness should be considered as a limiting factor for legend design [50], and to the extent possible, researchers should attempt to use categories that are supported by both the spatial resolution of the model data and the field sampling protocols to be used; we recommend that researchers consult the extensive literature on legend design [22,138–141,206–208].

### *4.3. Step 3: Minimize collection-related errors*

There are numerous ways to collect TD for categorical and continuous mapping projects, each with their own sources of error. There are thus many potential approaches for minimizing the associated collection errors, which may be quite specific to a particular variable [e.g. for agricultural area estimates 209]. However, there are several general approaches that can be followed to minimize TD collection errors. Our focus here is primarily on error in image-interpreted TD, which is one of the most common approaches used to training ML mapping algorithms. We also touch on the specific case of model-derived training data.

Whenever possible, we recommend using protocols that incorporate training reference data to independently assess TD accuracy, particularly for image-interpreted TD [e.g. 144]. Training reference datasets can be limited in size compared to the ultimate sample size, provided that training reference locations are randomly presented to interpreters during the data creation campaign [144]. Active feedback during training label creation can also help reduce errors on a rolling basis, by providing interpreters information regarding their performance [169].

If comparison against training reference data is not possible, then consensus methods for generating TD may be the next best alternative. Consensus among several domain experts may also be the best and most practical measure for collecting both training reference data and map reference data [31,54]. In the case of image-interpreted samples, consensus approaches should employ multiple interpreters to label the same site. For continuous variables, several independent or repeated *in situ*

892 measurements should be made and averaged. For modeled variables where the error is unknown, as
893 in the surface flux case study, training based on the outputs of multiple independent models is
894 recommended. The agricultural case study shows how multiple mappings can be used to quantify
895 label uncertainty (Figure 12A) and minimize the amount of labeling error, which manifests through
896 improved map accuracy (Figure 11A). The surface flux case study demonstrates these same benefits
897 across several continuous variables (Figure 10). The number of separate measures or interpreters to
898 use will vary depending on the application. Some guidance for image-interpreted tasks comes from
899 the land cover accuracy assessment literature, where consensus between at least 3 interpreters is
900 recommended to allow for majority voting [31,43], but more complex land covers may need up to 7
901 interpreters [43]. In the cropland mapping case study, 5 interpreters labelled each consensus training
902 sample. For the continuous surface flux example, 3 separate modeled inputs were used.
903 Further steps can be taken to minimize TD collection errors arising from image interpretation.
904 Interpreters should be given thorough training regarding the task [31], which may include instruction
905 on remote sensing principles as well as local or regional contextual information. Local domain
906 expertise is particularly helpful for consistent identification of idiosyncratic land covers [158].
907 Interpreter education is particularly important for crowdsourcing or citizen science data collection
908 campaigns, as participants typically lack formal experience in image interpretation [145,210].
909 As described in Step 2 above, image interpretation is inadvisable when the available imagery
910 does not support the legend categories in terms of spatial, spectral, temporal, or radiometric
911 resolution [211–213]. Researchers must be especially cautious in the similar but potentially more
912 hazardous case that HR/VHR imagery is used to create training samples that are then used with
913 coarser resolution imagery when ingested into the ML model. Assuming that researchers correctly
914 specify their data selection and legend design when using higher spatial resolution imagery to create
915 TD, image interpretation errors due to insufficient resolution should be minimized; however, special
916 care should be given to borderline classes, or classes exhibiting a high degree of spatial and/or
917 spectral variability due to land cover mixtures within the pixel [121,131,132,148,214]. In such cases,
918 we recommend that training polygons be created near the center of scene objects, where pixel mixing
919 is likely to be minimized [e.g. 52].
920 Another important error-minimizing approach relates to cases where TD comes from a process
921 model, as in the surface flux example outlined above. Process models are also increasingly used to
922 train crop yield mapping models, due to the difficulty of obtaining sufficiently large and reliable
923 field-scale yield data for training [215]. To circumvent this challenge, the Scalable Yield Mapping
924 (SCYM) method [216,217] uses a mechanistic crop model to simulate yields under various
925 environmental and management conditions. The model's outputs then become inputs for training an
926 empirical mapping model (typically ML), in which the simulated yield is the dependent variable and
927 a subset of remotely retrievable model variables serve as predictors. TD errors in such cases can be
928 minimized by rigorously calibrating the process model (itself a challenging task) using best practices
929 from the relevant modeling literature [e.g. 218]. Alternatively, if modeled TD are necessary but
930 careful calibration is not possible (e.g. because the data are pre-existing), then a merging approach
931 such as Triple Collocation (Section 4.2) can help reduce training error.

932 *4.4. Step 4. Assess error in training data error*

933 The best way to assess both TD (and map reference data) error is to measure it directly. For
934 continuous variables, calculating measurement error should be possible in many cases, even for
935 model-generated data, in which the variance can be calculated from simulation treatments [e.g. 218].
936 For categorical mapping, label error can be measured using an internal accuracy assessment protocol
937 that makes use of predefined training reference data (e.g. Estes et al., [144]).
938 However, it can be challenging to produce training reference data, and indeed in some cases the
939 true category is not clear, whether looking at an image or standing on site. In these cases, or when a
940 direct TD error measurement protocol is not available, we recommend that researchers calculate
941 uncertainty estimates based on repeated measures or multiple interpreter approaches [e.g. the crowd
942 standard deviation; 145] described in Step 3 above (and see Figure 12); this is useful for both training

and map reference data. We also recommend that additional measures relating to data collection speed, precision, and consistency be collected for individual data creators, as these can generate further insight into relative TD errors. This recommendation is based on experience in crowdsourced data creation [144,145], but it is applicable to any type of data collection, and could greatly bolster the understanding and quantification of error propagation.

If it is not possible to either directly quantify or TD error or relative uncertainty, then mapmakers should at a minimum clearly document the data creation methods, and detail likely sources of error and potential uncertainties.

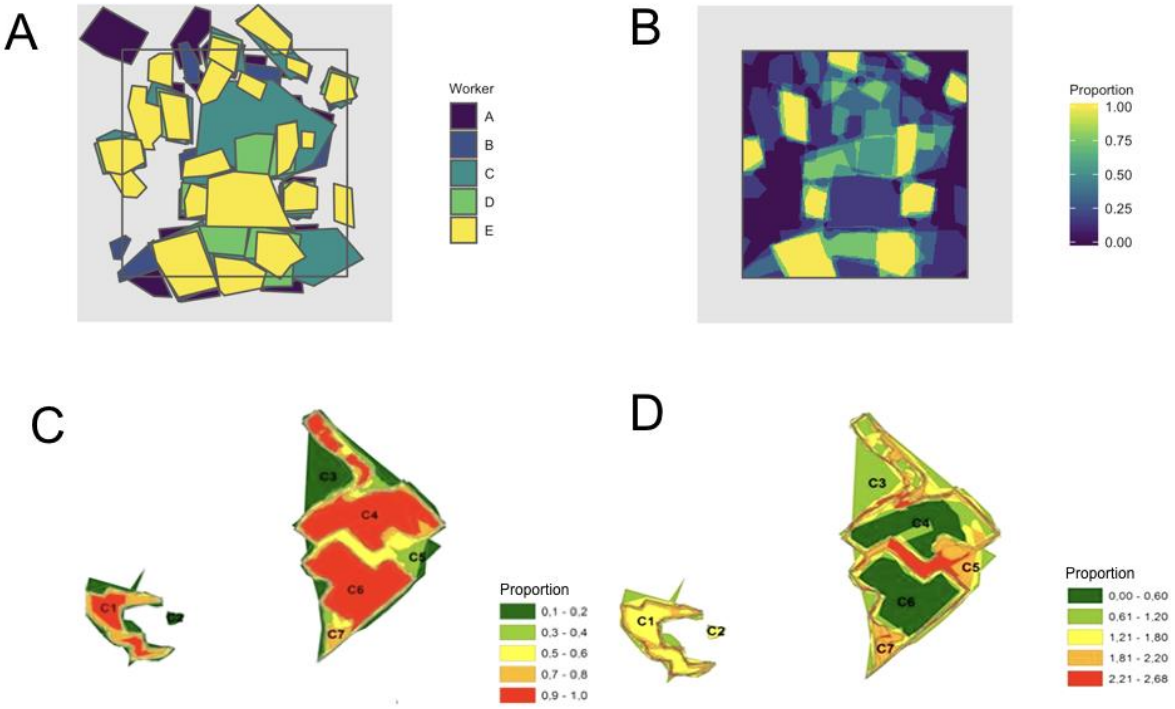


**Figure 12**: Two examples of consensus-based mapping approaches and their potential use for assessing training (or reference) data uncertainty. Panel A shows a collection of crop field boundary polygons drawn by five independent workers around crop fields visible in PlanetScope imagery collected over Ghana. These labels can be converted into a heat map (B) showing the overall agreement, the inverse of uncertainty. Similarly, 19 independent experts were asked to delineate slum settlements in image subset from Cape Town, South Africa. The polygons are converted into overall agreement and the uncertainty is modeled using random sets (C) shows the covering function, which is then used to calculate standard deviation of random set (D). Both these metrics indicate the variability as well as stability in boundaries delineated by different experts. Adapted with permission from Kohli et al. (2016).

### *4.5. Step 5. Evaluate and communicate the impact of training data error*

#### 4.5.1 TD Treatment Tiers

Due to the wide range of remote sensing research currently underway, a wide variety of TD and classification algorithms are in use. Therefore, it is not possible to specify a single protocol for treatment of TD error. Instead, we outline three tiers that represent different levels of accounting for the impact of TD errors on resulting map products. These three tiers presuppose that mapmakers follow best practices for map accuracy assessment, which includes selecting the most appropriate, literature-recommended accuracy measure(s), quantifying map reference sample error, and accounting for the impact of map reference data error on the accuracy measures (per Step 1). If these best practices are followed, TD error impacts will already be implicitly accounted for within the

accuracy measures, and the selected TD accounting tier will be governed by the purposes of the mapping application.

Tier 1

The optimal TD accuracy assessment, termed Tier 1, involves quantifying TD error using gold standard training reference data (Step 4), and then using that information to quantify varying aspects of TD sample (e.g. class balance, sample size) and collection error (label or measurement error) on model uncertainty and map accuracy, as several initial studies have demonstrated (see Sections 1.2.2 and 2.2). For example, the impact of TD error on the certainty of RandomForest classifications can be assessed using measures derived from the margin function [45]. The impact of TD error on map accuracy should also be assessed by training models with TD adjusted to reflect the range of measured TD error, as in our cropland mapping case study, and with respect to variations in TD sample size and class balance [27,e.g. 45,143]. This approach can be used to inform a mapmaker how much map improvement can be obtained by improving TD quality. As such, such tests should be performed against the validation sample to preserve the independence of map reference data.

We recommend that developers of benchmark TD libraries adhere to these guidelines. Undertaking such evaluations can provide users important information about appropriate usage of these data for different ML models and application within different mapping geographies. A rigorous quantification of error in the samples themselves is particularly important, since such data are also likely to be used as map reference data. Ideally, this tier should also be followed by the makers of map products intended for widespread public use, along with the release of TD and map reference data that were used [54]. This step would allow users full insight into the quality and usability of the map for their own purposes.

Published TD (and map reference data) should be documented with standard metadata, as shown in Table S3, including the relevant error metric associated with each observation. The SpatioTemporal Asset Catalog (STAC[7]) provides a framework for standardization of metadata for EO data and is increasingly seen as an international standard for geospatial data.

Tier 2

If it is not possible to directly measure and quantify TD error, the next best approach to account for TD error is to introduce a plausible range of simulated error into the TD and evaluate its impact on model uncertainty and map accuracy after training separate models with the perturbed datasets [e.g. 45]. If multiple workers are tasked with collecting TD for the same site, then the variance in their data can be calculated [e.g. 145] and derive the uncertainty bounds (e.g. Figure 12). This approach is demonstrated in the building mapping case study (section 4.1.1), which illustrates the sensitivity of key accuracy metrics to two different kinds of simulated labelling errors. The wheat yield case study (see section 4.3) provides an example of this approach for a continuous variable.

This tier may also provide an acceptable standard for both benchmark datasets and publicly released map products, particularly where absolute error quantification is less important, as well as for publicly released map products. TD and map reference data should also be made openly available with standard metadata, as described above, including the uncertainty metric for each observation. If it is not possible to publish them (e.g. because of privacy concerns), then researchers should accompany documentation that summarizes these data and their uncertainty.

Tier 3

If the TD error quantification in Tiers 1 or 2 are not possible, then mapmakers should publish their TD and map reference data [e.g., 52] with accompanying metadata that includes descriptions of potential errors and uncertainties. If data cannot be made open, then researchers should at a minimum publish full descriptions of the potential error in the data. Adherence to this tier, at least

[7] https://stacspec.org/

the reporting component, should be the minimal standard practice in peer-reviewed, map-based scientific research.

#### 4.5.1 Communicating error

Finally, uncertainty in ML-generated maps associated with both TD and map reference error should be faithfully reported within the maps and accompanying documents. Incomplete error reporting serves to limit the scientific validity and usefulness of these products [54]. Given that ML-generated maps are increasingly used by the public and policy domains, we advise makers of widely used maps to communicate these uncertainties and their consequences in a manner that is clear and understandable for broad, including non-specialist, audiences, so that users can understand the map and its limitations. In general, we recommend including the error on or as close to the actual map whenever possible, whether by means of metrics, the error matrix, and/or by using cartographic techniques for representing uncertainty. Examples of effective cartographic techniques for conveying uncertainty include selection of appropriate, intuitive, and color-blind friendly color schemes for classes and symbols, varying color value and saturation and font/line weight to indicate levels of uncertainty, use of crisp versus blurred boundaries and symbols to indicate the range of uncertainty, or display of consensus maps or side-by-side juxtaposition in cases of multiple, mutually exclusive predictions for the same place and time (e.g. representing differently specified models) [39,40]. Maps of consensus in training labels can provide valuable uncertainty information to users, such as shown in Figure 12A-B.

#### 4.5.2 Towards an Open Training Data Repository

For the scientific community, the ideal standard of openness and replicability is to provide a complete description of TD collection practices, appropriate accuracy metrics, and perhaps most importantly of all, the raw data. Ideally, we recommend the creation of a centralized, open source database of all available and relevant TD, using the details collected in the proposed template (Table S2), and recorded using the STAC framework. This type of open repository, taking inspiration from similar large-scale databases for computer vision [ImageNet, 219,SIFT10M Dataset, 220], and remote sensing [DeepSat, 221,UC Merced Land Use Dataset, 222], should contain full training metadata, citations to the peer-reviewed literature, as well as links to downloadable versions of TD collection protocols. Following the philosophy of free and open source software, we strongly recommend that researchers embrace open source data, which is the only way by which a study can be truly reproduced.

## 5. Conclusions

Current practices in EO research are generally inattentive to the need to evaluate and communicate the impact of TD error on ML-generated maps. This oversight undermines the goals of scientific reproducibility and may compromise the insights drawn from the resulting maps. Improving these practices is important given the increasing use of TD-intensive ML algorithms, which is the goal of our review and its resulting recommendations.

To resolve terminological differences introduced arising from the influence of non-EO disciplines, and to help contextualize training considerations relative to established map accuracy assessment practice, we distinguish between four types of "truth" data used in ML-based mapping projects (training, validation, training reference, and map reference data), and define the appropriate role for each (Section 1.2). We identify causes of error in TD as well as map reference data, distinguishing where these vary (Section 2.1), and then assess the impacts of TD error (Section 2.2), using a set of cases studies to illustrate the consequences TD error across a range of ML-based mapping applications (Section 3).

We then provide a set of guidelines for minimizing error arising from the design and collection of TD samples, and recommendations for measuring and accounting for the impact of these errors (Section 4). Many of these guidelines and procedures also relate to map reference data generation,

and we ground our recommendations in the existing best practices for map accuracy assignment (Sections 1.2.1 and 4.1). We conclude by defining three tiers of TD error accounting and reporting standards, which are designed for different kinds of ML-based mapping projects. The highest tiers should be adopted when creating open training libraries and public map products. Both kinds of datasets are increasingly being developed to meet the growing demand for EO-derived maps, and to deal with the growing complexity of EO mapping models. With respect to the latter, there is a pressing need to rigorously evaluate the training requirements and relative performance of deep learning models as they become more widely used for EO [33]. This need may be particularly great for continuous variable applications in Earth System Sciences, such as for hydrological research [223]. Training datasets that adhere to our suggested accounting standards will help to facilitate such model comparisons. If adopted within the peer-reviewed literature, these standards may also improve confidence in scientific findings drawn from map-based research, which can be confounded by poorly quantified map errors [30,54].

**Author Contributions:** This article synthesizes the ideas of the 20 authors resulting from a workshop focused on issues of error in training data for Machine Learning approaches in Earth Observation research. Conceptualization, L.E. and A.E.; formal analysis and investigation, L.E., H.A., R.A., J.R.E, L.F., D.K., D.L., A.R., L.S., S.Y., Z.Y.; writing—original draft preparation, A.E., L.E., H.A., L.F., D.K., D.L., R.G.P., A.R., Z.Y.; writing—review and editing, A.E., L.E., K.C., H.A., R.A., L.F., M.F., M.J., D.K., J.C.L.B., J.M., J.R.; visualization, H.A., R.A., L.F. D.K, A.R., H.S.; supervision, L.E.; project administration, L.E. and A.E.; funding acquisition, L.E., A. R. All authors have read and agreed to the published version of the manuscript.

## Acknowledgements

This work represents a synthesis of findings from a workshop held at Clark University on January 8-9, 2019. The workshop and subsequent paper writing and development was supported by a grant from Omidyar Network's Property Rights Initiative, now PlaceFund. Additional support for developing methods and data presented here was provided by NASA (80NSSC18K0158), the National Science Foundation (SES-1801251), National Institute of Standards and Technology (2017-67003-26615), National Institute of Standards and Technology Summer Undergraduate Research Fellowship Program, and New York State Department of Environmental Conservation (DEC01-T00640GG-3350000). We thank Victoria Gammino for helpful input and advice, and David Allen, Ayo Deas, Lucy Hutyra, Clare Kohler, Barry Logan, Jaret Reblin, Ian Smith for assistance with fieldwork and data compilation.

## References


1. Chen, J.; Chen, J.; Liao, A.; Cao, X.; Chen, L.; Chen, X.; He, C.; Han, G.; Peng, S.; Lu, M.; et al. Global Land Cover Mapping at 30 m Resolution: A POK-Based Operational Approach. *ISPRS J. Photogramm. Remote Sens.* **2015**, *103*, 7–27.
2. Friedl, M.A.; Sulla-Menashe, D.; Tan, B.; Schneider, A.; Ramankutty, N.; Sibley, A.; Huang, X. MODIS Collection 5 global land cover: Algorithm refinements and characterization of new datasets. *Remote Sens. Environ.* **2010**, *114*, 168–182.
3. Song, X.-P.; Hansen, M.C.; Stehman, S.V.; Potapov, P.V.; Tyukavina, A.; Vermote, E.F.; Townshend, J.R. Global land change from 1982 to 2016. *Nature* **2018**, *560*, 639–643.
4. Mohanty, B.P.; Cosh, M.H.; Lakshmi, V.; Montzka, C. Soil Moisture Remote Sensing: State-of-the-Science. *Vadose Zone J.* **2017**, *16*.
5. Daudt, R.C.; Le Saux, B.; Boulch, A.; Gousseau, Y. Guided Anisotropic Diffusion and Iterative Learning for Weakly Supervised Change Detection. *arXiv [cs.CV]* 2019.
6. Hecht, R.; Meinel, G.; Buchroithner, M. Automatic identification of building types based on topographic databases – a comparison of different data sources. *International Journal of Cartography* **2015**, *1*, 18–31.
7. Zhang, X.; Jayavelu, S.; Liu, L.; Friedl, M.A.; Henebry, G.M.; Liu, Y.; Schaaf, C.B.; Richardson, A.D.; Gray, J. Evaluation of land surface phenology from VIIRS data using time series of PhenoCam imagery. *Agric. For. Meteorol.* **2018**, *256-257*, 137–149.
8. Tan, B.; Morisette, J.T.; Wolfe, R.E.; Gao, F.; Ederer, G.A.; Nightingale, J.; Pedelty, J.A. An Enhanced TIMESAT Algorithm for Estimating Vegetation Phenology Metrics From MODIS Data. *IEEE Journal of Selected Topics in Applied Earth Observations and Remote Sensing* **2011**, *4*, 361–371.
9. Zhang, X.; Friedl, M.A.; Schaaf, C.B. Global vegetation phenology from Moderate Resolution Imaging Spectroradiometer (MODIS): Evaluation of global patterns and comparison with in situ measurements: GLOBAL PHENOLOGY FROM MODIS. *J. Geophys. Res.* **2006**, *111*, 981.
10. Wan, Z. New refinements and validation of the MODIS Land-Surface Temperature/Emissivity products. *Remote Sens. Environ.* **2008**, *112*, 59–74.
11. Jiménez-Muñoz, J.C.; Sobrino, J.A.; Skoković, D.; Mattar, C.; Cristóbal, J. Land Surface Temperature Retrieval Methods From Landsat-8 Thermal Infrared Sensor Data. *IEEE Geoscience and Remote Sensing Letters* **2014**, *11*, 1840–1843.
12. Jean, N.; Burke, M.; Xie, M.; Davis, W.M.; Lobell, D.B.; Ermon, S. Combining satellite imagery and machine learning to predict poverty. *Science* **2016**, *353*, 790–794.
13. Pekel, J.-F.; Cottam, A.; Gorelick, N.; Belward, A.S. High-resolution mapping of global surface water and its long-term changes. *Nature* **2016**, *540*, 418–422.
14. Hansen, M.C.; Potapov, P.; Tyukavina, A. Comment on "Tropical forests are a net carbon source based on aboveground measurements of gain and loss." *Science* **2019**, *363*.
15. Gutierrez-Velez, V.H.; Pontius, R.G. Influence of carbon mapping and land change modelling on the prediction of carbon emissions from deforestation. *Environ. Conserv.* **2012**, *39*, 325–336.
16. Deng, J.; Dong, W.; Socher, R.; Li, L.-J.; Li, K.; Fei-Fei, L. Imagenet: A large-scale hierarchical image database. In Proceedings of the 2009 IEEE conference on computer vision and pattern recognition; Ieee, 2009; pp. 248–255.
17. Helber, P.; Bischke, B.; Dengel, A.; Borth, D. EuroSAT: A Novel Dataset and Deep Learning Benchmark for Land Use and Land Cover Classification. *IEEE Journal of Selected Topics in Applied Earth Observations and Remote Sensing* **2019**, 1–10.
18. Liu, Q.; Hang, R.; Song, H.; Li, Z. Learning Multiscale Deep Features for High-Resolution Satellite Image Scene Classification. *IEEE Trans. Geosci. Remote Sens.* **2018**, *56*, 117–126.
19. Laso Bayas, J.C.; Lesiv, M.; Waldner, F.; Schucknecht, A.; Duerauer, M.; See, L.; Fritz, S.; Fraisl, D.; Moorthy, I.; McCallum, I.; et al. A global reference database of crowdsourced cropland data collected using the Geo-Wiki platform. *Sci Data* **2017**, *4*, 170136.
20. Lary, D.J.; Zewdie, G.K.; Liu, X.; Wu, D.; Levetin, E.; Allee, R.J.; Malakar, N.; Walker, A.; Mussa, H.; Mannino, A.; et al. Machine Learning Applications for Earth Observation. In *Earth Observation Open Science and Innovation*; Mathieu, P.-P., Aubrecht, C., Eds.; Springer

International Publishing: Cham, 2018; pp. 165–218 ISBN 9783319656335.

21. Lary, D.J.; Alavi, A.H.; Gandomi, A.H.; Walker, A.L. Machine learning in geosciences and remote sensing. *Geoscience Frontiers* **2016**, *7*, 3–10.
22. Loveland, T.R.; Reed, B.C.; Brown, J.F.; Ohlen, D.O.; Zhu, Z.; Yang, L.; Merchant, J.W. Development of a global land cover characteristics database and IGBP DISCover from 1 km AVHRR data. *Int. J. Remote Sens.* **2000**, *21*, 1303–1330.
23. Sulla-Menashe, D.; Gray, J.M.; Abercrombie, S.P.; Friedl, M.A. Hierarchical mapping of annual global land cover 2001 to present: The MODIS Collection 6 Land Cover product. *Remote Sens. Environ.* **2019**, *222*, 183–194.
24. Fortier, J.; Rogan, J.; Woodcock, C.E.; Runfola, D.M. Utilizing Temporally Invariant Calibration Sites to Classify Multiple Dates and Types of Satellite Imagery. *Photogrammetric Engineering & Remote Sensing* **2011**, *77*, 181–189.
25. Foody, G.M.; Mathur, A. Toward intelligent training of supervised image classifications: directing training data acquisition for SVM classification. *Remote Sens. Environ.* **2004**, *93*, 107–117.
26. Graves, S.J.; Asner, G.P.; Martin, R.E.; Anderson, C.B.; Colgan, M.S.; Kalantari, L.; Bohlman, S.A. Tree Species Abundance Predictions in a Tropical Agricultural Landscape with a Supervised Classification Model and Imbalanced Data. *Remote Sensing* **2016**, *8*, 161.
27. Foody, G.; Pal, M.; Rocchini, D.; Garzon-Lopez, C. The sensitivity of mapping methods to reference data quality: Training supervised image classifications with imperfect reference data. *International Journal of ...* **2016**.
28. Maxwell, A.E.; Warner, T.A.; Fang, F. Implementation of machine-learning classification in remote sensing: an applied review. *Int. J. Remote Sens.* **2018**, *39*, 2784–2817.
29. Huang, C.; Davis, L.S.; Townshend, J.R.G. An assessment of support vector machines for land cover classification. *Int. J. Remote Sens.* **2002**, *23*, 725–749.
30. Estes, L.; Chen, P.; Debats, S.; Evans, T.; Ferreira, S.; Kuemmerle, T.; Ragazzo, G.; Sheffield, J.; Wolf, A.; Wood, E.; et al. A large-area, spatially continuous assessment of land cover map error and its impact on downstream analyses. *Glob. Chang. Biol.* **2018**, *24*, 322–337.
31. Pengra, B.W.; Stehman, S.V.; Horton, J.A.; Dockter, D.J.; Schroeder, T.A.; Yang, Z.; Cohen, W.B.; Healey, S.P.; Loveland, T.R. Quality control and assessment of interpreter consistency of annual land cover reference data in an operational national monitoring program. *Remote Sens. Environ.* **2019**, 111261.
32. Zhu, X.X.; Tuia, D.; Mou, L.; Xia, G.; Zhang, L.; Xu, F.; Fraundorfer, F. Deep Learning in Remote Sensing: A Comprehensive Review and List of Resources. *IEEE Geoscience and Remote Sensing Magazine* **2017**, *5*, 8–36.
33. Ma, L.; Liu, Y.; Zhang, X.; Ye, Y.; Yin, G.; Johnson, B.A. Deep learning in remote sensing applications: A meta-analysis and review. *ISPRS J. Photogramm. Remote Sens.* **2019**, *152*, 166–177.
34. Foody, G.M. Status of land cover classification accuracy assessment. *Remote Sens. Environ.* **2002**, *80*, 185–201.
35. Foody, G.M. Assessing the accuracy of land cover change with imperfect ground reference data. *Remote Sensing of Environment* 2010, *114*, 2271–2285.
36. Olofsson, P.; Foody, G.M.; Herold, M.; Stehman, S.V.; Woodcock, C.E.; Wulder, M.A. Good practices for estimating area and assessing accuracy of land change. *Remote Sens. Environ.* **2014**, *148*, 42–57.
37. Pontius, R.G.; Millones, M. Death to Kappa: birth of quantity disagreement and allocation disagreement for accuracy assessment. *Int. J. Remote Sens.* **2011**, *32*, 4407–4429.
38. Congalton, R.G.; Green, K. *Assessing the accuracy of remotely sensed data: principles and practices*; CRC press, 2008;.
39. Monmonier, M. Cartography: uncertainty, interventions, and dynamic display. *Prog. Hum. Geogr.* **2006**, *30*, 373–381.
40. MacEachren, A.M. Visualizing Uncertain Information. *1* **1992**, 10–19.
41. Goodchild, M.F.; Gopal, S. *The Accuracy Of Spatial Databases*; CRC Press, 1989; ISBN 9780203490235.
42. Congalton, R.G. A review of assessing the accuracy of classifications of remotely sensed data. *Remote Sens. Environ.* **1991**, *37*, 35–46.

43. McRoberts, R.E.; Stehman, S.V.; Liknes, G.C.; Næsset, E.; Sannier, C.; Walters, B.F. The effects of imperfect reference data on remote sensing-assisted estimators of land cover class proportions. *ISPRS J. Photogramm. Remote Sens.* **2018**, *142*, 292–300.
44. Carlotto, M.J. Effect of errors in ground truth on classification accuracy. *Int. J. Remote Sens.* **2009**, *30*, 4831–4849.
45. Mellor, A.; Boukir, S.; Haywood, A.; Jones, S. Exploring issues of training data imbalance and mislabelling on random forest performance for large area land cover classification using the ensemble margin. *ISPRS J. Photogramm. Remote Sens.* **2015**, *105*, 155–168.
46. Swan, B.; Laverdiere, M.; Yang, H.L. How Good is Good Enough?: Quantifying the Effects of Training Set Quality. In Proceedings of the Proceedings of the 2Nd ACM SIGSPATIAL International Workshop on AI for Geographic Knowledge Discovery; ACM: New York, NY, USA, 2018; pp. 47–51.
47. Ghimire, B.; Rogan, J.; Galiano, V.R.; Panday, P.; Neeti, N. An Evaluation of Bagging, Boosting, and Random Forests for Land-Cover Classification in Cape Cod, Massachusetts, USA. *GISci. Remote Sens.* **2012**, *49*, 623–643.
48. Rodriguez-Galiano, V.F.; Ghimire, B.; Rogan, J.; Chica-Olmo, M.; Rigol-Sanchez, J.P. An assessment of the effectiveness of a random forest classifier for land-cover classification. *ISPRS J. Photogramm. Remote Sens.* **2012**, *67*, 93–104.
49. Bruzzone, L.; Persello, C. A Novel Context-Sensitive Semisupervised SVM Classifier Robust to Mislabeled Training Samples. *IEEE Trans. Geosci. Remote Sens.* **2009**, *47*, 2142–2154.
50. Cracknell, M.J.; Reading, A.M. Geological mapping using remote sensing data: A comparison of five machine learning algorithms, their response to variations in the spatial distribution of training data and the use of explicit spatial information. *Comput. Geosci.* **2014**, *63*, 22–33.
51. Mellor, A.; Boukir, S. Exploring diversity in ensemble classification: Applications in large area land cover mapping. *ISPRS J. Photogramm. Remote Sens.* **2017**, *129*, 151–161.
52. Xiong, J.; Thenkabail, P.S.; Tilton, J.C.; Gumma, M.K.; Teluguntla, P.; Oliphant, A.; Congalton, R.G.; Yadav, K.; Gorelick, N. Nominal 30-m Cropland Extent Map of Continental Africa by Integrating Pixel-Based and Object-Based Algorithms Using Sentinel-2 and Landsat-8 Data on Google Earth Engine. *Remote Sensing* **2017**, *9*, 1065.
53. Bey, A.; Jetimane, J.; Lisboa, S.N.; Ribeiro, N.; Sitoe, A.; Meyfroidt, P. Mapping smallholder and large-scale cropland dynamics with a flexible classification system and pixel-based composites in an emerging frontier of Mozambique. *Remote Sens. Environ.* **2020**, *239*, 111611.
54. Stehman, S.V.; Foody, G.M. Key issues in rigorous accuracy assessment of land cover products. *Remote Sens. Environ.* **2019**, *231*, 111199.
55. Zhang, C.; Xie, Z. Object-based Vegetation Mapping in the Kissimmee River Watershed Using HyMap Data and Machine Learning Techniques. *Wetlands* **2013**, *33*, 233–244.
56. Rogan, J.; Franklin, J.; Stow, D.; Miller, J.; Woodcock, C.; Roberts, D. Mapping land-cover modifications over large areas: A comparison of machine learning algorithms. *Remote Sens. Environ.* **2008**, *112*, 2272–2283.
57. Copass, C.; Antonova, N.; Kennedy, R. Comparison of Office and Field Techniques for Validating Landscape Change Classification in Pacific Northwest National Parks. *Remote Sensing* **2018**, *11*, 3.
58. Lesiv, M.; See, L.; Laso Bayas, J.C.; Sturn, T.; Schepaschenko, D.; Karner, M.; Moorthy, I.; McCallum, I.; Fritz, S. Characterizing the Spatial and Temporal Availability of Very High Resolution Satellite Imagery in Google Earth and Microsoft Bing Maps as a Source of Reference Data. *Land* **2018**, *7*, 118.
59. Biradar, C.M.; Thenkabail, P.S.; Noojipady, P.; Li, Y.; Dheeravath, V.; Turral, H.; Velpuri, M.; Gumma, M.K.; Gangalakunta, O.R.P.; Cai, X.L.; et al. A global map of rainfed cropland areas (GMRCA) at the end of last millennium using remote sensing. *Int. J. Appl. Earth Obs. Geoinf.* **2009**, *11*, 114–129.
60. Mallinis, G.; Emmanoloudis, D.; Giannakopoulos, V.; Maris, F.; Koutsias, N. Mapping and interpreting historical land cover/land use changes in a Natura 2000 site using earth observational data: The case of Nestos delta, Greece. *Appl. Geogr.* **2011**, *31*, 312–320.
61. Jawak, S.D.; Luis, A.J. Improved land cover mapping using high resolution multiangle 8-band WorldView-2 satellite remote sensing data. *JARS* **2013**, *7*, 073573.
62. Ye, S.; Pontius, R.G.; Rakshit, R. A review of accuracy assessment for object-based image

analysis: From per-pixel to per-polygon approaches. *ISPRS J. Photogramm. Remote Sens.* **2018**, *141*, 137–147.
63. Fritz, S.; See, L.; Perger, C.; McCallum, I.; Schill, C.; Schepaschenko, D.; Duerauer, M.; Karner, M.; Dresel, C.; Laso-Bayas, J.-C.; et al. A global dataset of crowdsourced land cover and land use reference data. *Sci Data* **2017**, *4*, 170075.
64. Stehman, S.V. Sampling designs for accuracy assessment of land cover. *Int. J. Remote Sens.* **2009**, *30*, 5243–5272.
65. Brodrick, P.G.; Davies, A.B.; Asner, G.P. Uncovering Ecological Patterns with Convolutional Neural Networks. *Trends Ecol. Evol.* **2019**, *34*, 734–745.
66. Xiao, T.; Xia, T.; Yang, Y.; Huang, C.; Wang, X. Learning from massive noisy labeled data for image classification. In Proceedings of the Proceedings of the IEEE conference on computer vision and pattern recognition; cv-foundation.org, 2015; pp. 2691–2699.
67. Frénay, B.; Verleysen, M. Classification in the presence of label noise: a survey. *IEEE Trans Neural Netw Learn Syst* **2014**, *25*, 845–869.
68. Brodley, C.E.; Friedl, M.A. Identifying Mislabeled Training Data. *1* **1999**, *11*, 131–167.
69. Van Etten, A.; Lindenbaum, D.; Bacastow, T.M. SpaceNet: A Remote Sensing Dataset and Challenge Series. *arXiv [cs.CV]* 2018.
70. Sumbul, G.; Charfuelan, M.; Demir, B.; Markl, V. BigEarthNet: A Large-Scale Benchmark Archive For Remote Sensing Image Understanding. *arXiv [cs.CV]* 2019.
71. Lesiv, M.; Laso Bayas, J.C.; See, L.; Duerauer, M.; Dahlia, D.; Durando, N.; Hazarika, R.; Kumar Sahariah, P.; Vakolyuk, M. 'yana; Blyshchyk, V.; et al. Estimating the global distribution of field size using crowdsourcing. *Glob. Chang. Biol.* **2019**, *25*, 174–186.
72. Fritz, S.; McCallum, I.; Schill, C.; Perger, C.; See, L.; Schepaschenko, D.; van der Velde, M.; Kraxner, F.; Obersteiner, M. Geo-Wiki: An Online Platform for Improving Global Land Cover. *Environmental Modelling & Software* **2012**, *31*, 110–123.
73. Goodchild, M.F. Citizens as sensors: the world of volunteered geography. *GeoJournal* **2007**, *69*, 211–221.
74. Kohavi, R.; Others A study of cross-validation and bootstrap for accuracy estimation and model selection. In Proceedings of the Ijcai; Montreal, Canada, 1995; Vol. 14, pp. 1137–1145.
75. Olofsson, P.; Foody, G.M.; Stehman, S.V.; Woodcock, C.E. Making better use of accuracy data in land change studies: Estimating accuracy and area and quantifying uncertainty using stratified estimation. *Remote Sens. Environ.* **2013**, *129*, 122–131.
76. Catal, C. Performance evaluation metrics for software fault prediction studies. *Acta Polytechnica Hungarica* **2012**, *9*, 193–206.
77. Stehman, S.V.; Foody, G.M. Key issues in rigorous accuracy assessment of land cover products. *Remote Sens. Environ.* **2019**, *231*, 111199.
78. Jeni, L.A.; Cohn, J.F.; De La Torre, F. Facing Imbalanced Data--Recommendations for the Use of Performance Metrics. In Proceedings of the 2013 Humaine Association Conference on Affective Computing and Intelligent Interaction; 2013; pp. 245–251.
79. Kuzera, K.; Pontius, R.G. Importance of Matrix Construction for Multiple-Resolution Categorical Map Comparison. *GISci. Remote Sens.* **2008**, *45*, 249–274.
80. Pontius, R.G.; Thontteh, O.; Chen, H. Components of information for multiple resolution comparison between maps that share a real variable. *Environ. Ecol. Stat.* **2008**, *15*, 111–142.
81. Pontius, R.G.; Parmentier, B. Recommendations for using the relative operating characteristic (ROC). *Landsc. Ecol.* **2014**, *29*, 367–382.
82. Pontius, R.G. Component intensities to relate difference by category with difference overall. *Int. J. Appl. Earth Obs. Geoinf.* **2019**, *77*, 94–99.
83. Pontius, R.G., Jr.; Connors, J. Range of Categorical Associations for Comparison of Maps with Mixed Pixels. *Photogrammetric Engineering & Remote Sensing* **2009**, *75*, 963–969.
84. Allouche, O.; Tsoar, A.; Kadmon, R. Assessing the Accuracy of Species Distribution Models: Prevalence, Kappa and the True Skill Statistic (TSS). *J. Appl. Ecol.* **2006**, *43*, 1223–1232.
85. Willmott, C.J.; Matsuura, K. On the use of dimensioned measures of error to evaluate the performance of spatial interpolators. *Int. J. Geogr. Inf. Sci.* **2006**, *20*, 89–102.
86. Willmott, C.J.; Matsuura, K.; Robeson, S.M. Ambiguities inherent in sums-of-squares-based error statistics. *Atmos. Environ.* **2009**, *43*, 749–752.
87. Willmott, C.J.; Matsuura, K. Advantages of the mean absolute error (MAE) over the root mean

square error (RMSE) in assessing average model performance. *Clim. Res.* **2005**, *30*, 79–82.
88. Pontius, R.G., Jr; Si, K. The total operating characteristic to measure diagnostic ability for multiple thresholds. *Int. J. Geogr. Inf. Sci.* **2014**, *28*, 570–583.
89. Fielding, A.H.; Bell, J.F. A review of methods for the assessment of prediction errors in conservation presence/absence models. *Environ. Conserv.* **1997**, *24*, 38–49.
90. Blaschke, T. Object based image analysis for remote sensing. *ISPRS J. Photogramm. Remote Sens.* **2010**, *65*, 2–16.
91. Costa, H.; Foody, G.M.; Boyd, D.S. Supervised methods of image segmentation accuracy assessment in land cover mapping. *Remote Sens. Environ.* **2018**, *205*, 338–351.
92. Olofsson, P.; Foody, G.M.; Herold, M.; Stehman, S.V.; Woodcock, C.E.; Wulder, M.A. Good Practices for Estimating Area and Assessing Accuracy of Land Change. *Remote Sens. Environ.* **2014**, *148*, 42–57.
93. Foody, G.M. Assessing the accuracy of land cover change with imperfect ground reference data. *Remote Sens. Environ.* **2010**, *114*, 2271–2285.
94. Zhong, B.; Ma, P.; Nie, A.; Yang, A.; Yao, Y.; Lü, W.; Zhang, H.; Liu, Q. Land cover mapping using time series HJ-1/CCD data. *Sci. China Earth Sci.* **2014**, *57*, 1790–1799.
95. Pacifici, F.; Chini, M.; Emery, W.J. A neural network approach using multi-scale textural metrics from very high-resolution panchromatic imagery for urban land-use classification. *Remote Sens. Environ.* **2009**, *113*, 1276–1292.
96. Abbas, I.I.; Muazu, K.M.; Ukoje, J.A.; Others Mapping land use-land cover and change detection in Kafur local government, Katsina, Nigeria (1995-2008) using remote sensing and GIS. *Research journal of environmental and Earth Sciences* **2010**, *2*, 6–12.
97. Sano, E.E.; Rosa, R.; Brito, J.L.S.; Ferreira, L.G. Land cover mapping of the tropical savanna region in Brazil. *Environ. Monit. Assess.* **2010**, *166*, 113–124.
98. Hu, T.; Yang, J.; Li, X.; Gong, P. Mapping Urban Land Use by Using Landsat Images and Open Social Data. *Remote Sensing* **2016**, *8*, 151.
99. Galletti, C.S.; Myint, S.W. Land-Use Mapping in a Mixed Urban-Agricultural Arid Landscape Using Object-Based Image Analysis: A Case Study from Maricopa, Arizona. *Remote Sensing* **2014**, *6*, 6089–6110.
100. Hu, Q.; Wu, W.; Xia, T.; Yu, Q.; Yang, P.; Li, Z.; Song, Q. Exploring the Use of Google Earth Imagery and Object-Based Methods in Land Use/Cover Mapping. *Remote Sensing* **2013**, *5*, 6026–6042.
101. Al-Bakri, J.T.; Ajlouni, M.; Abu-Zanat, M. Incorporating Land Use Mapping and Participation in Jordan: An Approach to Sustainable Management of Two Mountainous Areas. *Mt. Res. Dev.* **2008**, *28*, 49–57.
102. Liu, J.; Kuang, W.; Zhang, Z.; Xu, X.; Qin, Y.; Ning, J.; Zhou, W.; Zhang, S.; Li, R.; Yan, C.; et al. Spatiotemporal characteristics, patterns, and causes of land-use changes in China since the late 1980s. *J. Geogr. Sci.* **2014**, *24*, 195–210.
103. Yadav, P.K.; Kapoor, M.; Sarma, K. Land Use Land Cover Mapping, Change Detection and Conflict Analysis of Nagzira-Navegaon Corridor, Central India Using Geospatial Technology. *International Journal of Remote Sensing and GIS* **2012**, *1*.
104. d. C. Freitas, C.; d. S. Soler, L.; Sant'Anna, S.J.S.; Dutra, L.V.; dos Santos, J.R.; Mura, J.C.; Correia, A.H. Land Use and Land Cover Mapping in the Brazilian Amazon Using Polarimetric Airborne P-Band SAR Data. *IEEE Trans. Geosci. Remote Sens.* **2008**, *46*, 2956–2970.
105. Dewan, A.M.; Yamaguchi, Y. Land use and land cover change in Greater Dhaka, Bangladesh: Using remote sensing to promote sustainable urbanization. *Appl. Geogr.* **2009**, *29*, 390–401.
106. Castañeda, C.; Ducrot, D. Land cover mapping of wetland areas in an agricultural landscape using SAR and Landsat imagery. *J. Environ. Manage.* **2009**, *90*, 2270–2277.
107. Griffiths, P.; van der Linden, S.; Kuemmerle, T.; Hostert, P. A Pixel-Based Landsat Compositing Algorithm for Large Area Land Cover Mapping. *IEEE Journal of Selected Topics in Applied Earth Observations and Remote Sensing* **2013**, *6*, 2088–2101.
108. Ge, Y. Sub-pixel land-cover mapping with improved fraction images upon multiple-point simulation. *Int. J. Appl. Earth Obs. Geoinf.* **2013**, *22*, 115–126.
109. Gong, P.; Wang, J.; Yu, L.; Zhao, Y.; Zhao, Y.; Liang, L.; Niu, Z.; Huang, X.; Fu, H.; Liu,

S.; et al. Finer resolution observation and monitoring of global land cover: first mapping results with Landsat TM and ETM+ data. *Int. J. Remote Sens.* **2013**, *34*, 2607–2654.
110. Ghorbani, A.; Pakravan, M. Land use mapping using visual vs. digital image interpretation of TM and Google earth derived imagery in Shrivan-Darasi watershed (Northwest of Iran).
111. Deng, J.S.; Wang, K.; Hong, Y.; Qi, J.G. Spatio-temporal dynamics and evolution of land use change and landscape pattern in response to rapid urbanization. *Landsc. Urban Plan.* **2009**, *92*, 187–198.
112. Otukei, J.R.; Blaschke, T. Land cover change assessment using decision trees, support vector machines and maximum likelihood classification algorithms. *Int. J. Appl. Earth Obs. Geoinf.* **2010**, *12*, S27–S31.
113. Malinverni, E.S.; Tassetti, A.N.; Mancini, A.; Zingaretti, P.; Frontoni, E.; Bernardini, A. Hybrid object-based approach for land use/land cover mapping using high spatial resolution imagery. *Int. J. Geogr. Inf. Sci.* **2011**, *25*, 1025–1043.
114. Rozenstein, O.; Karnieli, A. Comparison of methods for land-use classification incorporating remote sensing and GIS inputs. *Appl. Geogr.* **2011**, *31*, 533–544.
115. Ran, Y.H.; Li, X.; Lu, L.; Li, Z.Y. Large-scale land cover mapping with the integration of multi-source information based on the Dempster–Shafer theory. *Int. J. Geogr. Inf. Sci.* **2012**, *26*, 169–191.
116. Clark, M.L.; Aide, T.M.; Grau, H.R.; Riner, G. A scalable approach to mapping annual land cover at 250 m using MODIS time series data: A case study in the Dry Chaco ecoregion of South America. *Remote Sens. Environ.* **2010**, *114*, 2816–2832.
117. Berberoglu, S.; Akin, A. Assessing different remote sensing techniques to detect land use/cover changes in the eastern Mediterranean. *Int. J. Appl. Earth Obs. Geoinf.* **2009**, *11*, 46–53.
118. Breiman, L. Random Forests. *Mach. Learn.* **2001**, *45*, 5–32.
119. Freeman, E.A.; Moisen, G.G.; Frescino, T.S. Evaluating effectiveness of down-sampling for stratified designs and unbalanced prevalence in Random Forest models of tree species distributions in Nevada. *Ecol. Modell.* **2012**, *233*, 1–10.
120. Townshend, J.R.; Masek, J.G.; Huang, C.; Vermote, E.F.; Gao, F.; Channan, S.; Sexton, J.O.; Feng, M.; Narasimhan, R.; Kim, D.; et al. Global characterization and monitoring of forest cover using Landsat data: opportunities and challenges. *International Journal of Digital Earth* **2012**, *5*, 373–397.
121. Shao, Y.; Lunetta, R.S. Comparison of support vector machine, neural network, and CART algorithms for the land-cover classification using limited training data points. *ISPRS J. Photogramm. Remote Sens.* **2012**, *70*, 78–87.
122. Planet Team Planet Application Program Interface: In Space for Life on Earth. San Francisco, CA 2017.
123. Manfreda, S.; McCabe, M.F.; Miller, P.E.; Lucas, R.; Pajuelo Madrigal, V.; Mallinis, G.; Ben Dor, E.; Helman, D.; Estes, L.; Ciraolo, G.; et al. On the Use of Unmanned Aerial Systems for Environmental Monitoring. *Remote Sensing* **2018**, *10*, 641.
124. Toutin, T. Geometric processing of IKONOS Geo images with DEM. In Proceedings of the Proceedings of ISPRS Joint Workshop “High Resolution Mapping from Space” 2001; pdfs.semanticscholar.org, 2001; pp. 19–21.
125. Reinartz, P.; Müller, R.; Schwind, P.; Suri, S.; Bamler, R. Orthorectification of VHR optical satellite data exploiting the geometric accuracy of TerraSAR-X data. *ISPRS J. Photogramm. Remote Sens.* **2011**, *66*, 124–132.
126. Aguilar, M.A.; Saldaña, M. del M.; Aguilar, F.J. Assessing geometric accuracy of the orthorectification process from GeoEye-1 and WorldView-2 panchromatic images. *Int. J. Appl. Earth Obs. Geoinf.* **2013**, *21*, 427–435.
127. Chen, J.; Zipf, A. DeepVGI: Deep Learning with Volunteered Geographic Information. In Proceedings of the Proceedings of the 26th International Conference on World Wide Web Companion; International World Wide Web Conferences Steering Committee: Republic and Canton of Geneva, Switzerland, 2017; pp. 771–772.
128. Kaiser, P.; Wegner, J.D.; Lucchi, A.; Jaggi, M.; Hofmann, T.; Schindler, K. Learning Aerial Image Segmentation From Online Maps. *IEEE Trans. Geosci. Remote Sens.* **2017**, *55*, 6054–6068.

129. Audebert, N.; Le Saux, B.; Lefèvre, S. Joint learning from earth observation and openstreetmap data to get faster better semantic maps. In Proceedings of the Proceedings of the IEEE Conference on Computer Vision and Pattern Recognition Workshops; 2017; pp. 67–75.
130. Strahler, A.H.; Woodcock, C.E.; Smith, J.A. On the nature of models in remote sensing. *Remote Sens. Environ.* **1986**, *20*, 121–139.
131. Foody, G.M. Relating the land-cover composition of mixed pixels to artificial neural network classification output. *Photogramm. Eng. Remote Sens.* **1996**, *62*, 491–498.
132. Moody, A.; Gopal, S.; Strahler, A.H. Artificial neural network response to mixed pixels in coarse-resolution satellite data. *Remote Sens. Environ.* **1996**, *58*, 329–343.
133. De Fries, R.S.; Hansen, M.; Townshend, J.R.G.; Sohlberg, R. Global land cover classifications at 8 km spatial resolution: The use of training data derived from Landsat imagery in decision tree classifiers. *Int. J. Remote Sens.* **1998**, *19*, 3141–3168.
134. Hansen, M.C.; Potapov, P.V.; Moore, R.; Hancher, M.; Turubanova, S.A.; Tyukavina, A.; Thau, D.; Stehman, S.V.; Goetz, S.J.; Loveland, T.R.; et al. High-resolution global maps of 21st-century forest cover change. *Science* **2013**, *342*, 850–853.
135. Kennedy, R.E.; Yang, Z.; Cohen, W.B. Detecting trends in forest disturbance and recovery using yearly Landsat time series: 1. LandTrendr — Temporal segmentation algorithms. *Remote Sens. Environ.* **2010**, *114*, 2897–2910.
136. Oppenshaw, S.; Taylor, P. A million or so correlation coefficients. *Statistical methods in the spatial sciences. Pion, London* **1979**.
137. Jelinski, D.E.; Wu, J. The modifiable areal unit problem and implications for landscape ecology. *Landsc. Ecol.* **1996**, *11*, 129–140.
138. Weiss, M.; de Beaufort, L.; Baret, F.; Allard, D.; Bruguier, N.; Marloie, O. Mapping leaf area index measurements at different scales for the validation of large swath satellite sensors: first results of the VALERI project. In Proceedings of the 8th International symposium in physical measurements and remote sensing, Aussois (France); w3.avignon.inra.fr, 2001; pp. 125–130.
139. Tian, Y.; Woodcock, C.E.; Wang, Y.; Privette, J.L.; Shabanov, N.V.; Zhou, L.; Zhang, Y.; Buermann, W.; Dong, J.; Veikkanen, B.; et al. Multiscale analysis and validation of the MODIS LAI product: I. Uncertainty assessment. *Remote Sens. Environ.* **2002**, *83*, 414–430.
140. Masuoka, E.; Roy, D.; Wolfe, R.; Morisette, J.; Sinno, S.; Teague, M.; Saleous, N.; Devadiga, S.; Justice, C.O.; Nickeson, J. MODIS Land Data Products: Generation, Quality Assurance and Validation. In *Land Remote Sensing and Global Environmental Change: NASA's Earth Observing System and the Science of ASTER and MODIS*; Ramachandran, B., Justice, C.O., Abrams, M.J., Eds.; Springer New York: New York, NY, 2011; pp. 509–531 ISBN 9781441967497.
141. Cohen, W.B.; Justice, C.O. Validating MODIS terrestrial ecology products: linking in situ and satellite measurements. *Remote Sens. Environ.* **1999**, *70*, 1–3.
142. Fritz, S.; See, L.; McCallum, I.; You, L.; Bun, A.; Moltchanova, E.; Duerauer, M.; Albrecht, F.; Schill, C.; Perger, C.; et al. Mapping global cropland and field size. *Glob. Chang. Biol.* **2015**, *21*, 1980–1992.
143. Debats, S.R.; Estes, L.D.; Thompson, D.R.; Caylor, K.K. *Integrating active learning and crowdsourcing into large-scale supervised landcover mapping algorithms*; PeerJ Preprints, 2017;.
144. Estes, L.D.; McRitchie, D.; Choi, J.; Debats, S.; Evans, T.; Guthe, W.; Luo, D.; Ragazzo, G.; Zempleni, R.; Caylor, K.K. A Platform for Crowdsourcing the Creation of Representative, Accurate Landcover Maps. *Environmental Modelling & Software* **2016**, *80*, 41–53.
145. Waldner, F.; Schucknecht, A.; Lesiv, M.; Gallego, J.; See, L.; Pérez-Hoyos, A.; d'Andrimont, R.; de Maet, T.; Bayas, J.C.L.; Fritz, S.; et al. Conflation of expert and crowd reference data to validate global binary thematic maps. *Remote Sens. Environ.* **2019**, *221*, 235–246.
146. Bey, A.; Sánchez-Paus Díaz, A.; Maniatis, D.; Marchi, G.; Mollicone, D.; Ricci, S.; Bastin, J.-F.; Moore, R.; Federici, S.; Rezende, M.; et al. Collect Earth: Land Use and Land Cover Assessment through Augmented Visual Interpretation. *Remote Sensing* **2016**, *8*, 807.
147. Fritz, S.; Sturn, T.; Karner, M.; Moorthy, I.; See, L.; Laso Bayas, J.C.; Fraisl, D. FotoQuest Go: A Citizen Science Approach to the Collection of In-Situ Land Cover and Land Use Data

for Calibration and Validation.; pure.iiasa.ac.at, 2019.
148. Tuia, D.; Pasolli, E.; Emery, W.J. Using active learning to adapt remote sensing image classifiers. *Remote Sensing of Environment* 2011, *115*, 2232–2242.
149. Powell, R.L.; Matzke, N.; de Souza, C.; Clark, M.; Numata, I.; Hess, L.L.; Roberts, D.A. Sources of error in accuracy assessment of thematic land-cover maps in the Brazilian Amazon. *Remote Sens. Environ.* **2004**, *90*, 221–234.
150. Van Coillie, F.M.B.; Gardin, S.; Anseel, F.; Duyck, W.; Verbeke, L.P.C.; De Wulf, R.R. Variability of operator performance in remote-sensing image interpretation: the importance of human and external factors. *Int. J. Remote Sens.* **2014**, *35*, 754–778.
151. Johnson, B.A.; Iizuka, K. Integrating OpenStreetMap crowdsourced data and Landsat time-series imagery for rapid land use/land cover (LULC) mapping: Case study of the Laguna de Bay area of the Philippines. *Appl. Geogr.* **2016**, *67*, 140–149.
152. Neigh, C.S.R.; Carroll, M.L.; Wooten, M.R.; McCarty, J.L.; Powell, B.F.; Husak, G.J.; Enenkel, M.; Hain, C.R. Smallholder crop area mapped with wall-to-wall WorldView sub-meter panchromatic image texture: A test case for Tigray, Ethiopia. *Remote Sens. Environ.* **2018**, *212*, 8–20.
153. Clark, M.L.; Aide, T.M.; Riner, G. Land change for all municipalities in Latin America and the Caribbean assessed from 250-m MODIS imagery (2001–2010). *Remote Sens. Environ.* **2012**, *126*, 84–103.
154. Comber, A.; Fisher, P. What is land cover? *Environment and Planning* **2005**.
155. Kohli, D.; Sliuzas, R.; Kerle, N.; Stein, A. An ontology of slums for image-based classification. *Comput. Environ. Urban Syst.* **2012**, *36*, 154–163.
156. Verburg, P.H.; Neumann, K.; Nol, L. Challenges in using land use and land cover data for global change studies. *Glob. Chang. Biol.* **2011**, *17*, 974–989.
157. Weng, Q. Remote sensing of impervious surfaces in the urban areas: Requirements, methods, and trends. *Remote Sens. Environ.* **2012**, *117*, 34–49.
158. Kohli, D.; Stein, A.; Sliuzas, R. Uncertainty analysis for image interpretations of urban slums. *Comput. Environ. Urban Syst.* **2016**, *60*, 37–49.
159. Rocchini, D. While Boolean sets non-gently rip: A theoretical framework on fuzzy sets for mapping landscape patterns. *Ecol. Complex.* **2010**, *7*, 125–129.
160. Woodcock, C.E.; Gopal, S. Fuzzy set theory and thematic maps: accuracy assessment and area estimation. *Int. J. Geogr. Inf. Sci.* **2000**, *14*, 153–172.
161. Rocchini, D.; Foody, G.M.; Nagendra, H.; Ricotta, C.; Anand, M.; He, K.S.; Amici, V.; Kleinschmit, B.; Förster, M.; Schmidtlein, S.; et al. Uncertainty in ecosystem mapping by remote sensing. *Comput. Geosci.* **2013**, *50*, 128–135.
162. Zhang, J.; Foody, G.M. A fuzzy classification of sub-urban land cover from remotely sensed imagery. *Int. J. Remote Sens.* **1998**, *19*, 2721–2738.
163. Woodcock, C.E.; Strahler, A.H. The factor of scale in remote sensing. *Remote Sens. Environ.* **1987**, *21*, 311–332.
164. Cracknell, A.P. Review article Synergy in remote sensing-what's in a pixel? *Int. J. Remote Sens.* **1998**, *19*, 2025–2047.
165. Pontius, R.G.; Cheuk, M.L. A generalized cross-tabulation matrix to compare soft-classified maps at multiple resolutions. *Int. J. Geogr. Inf. Sci.* **2006**, *20*, 1–30.
166. Silván-Cárdenas, J.L.; Wang, L. Sub-pixel confusion–uncertainty matrix for assessing soft classifications. *Remote Sens. Environ.* **2008**, *112*, 1081–1095.
167. Foody, G.M. The continuum of classification fuzziness in thematic mapping. *Photogramm. Eng. Remote Sens.* **1999**, *65*, 443–452.
168. Foody, G.M. Fully fuzzy supervised classification of land cover from remotely sensed imagery with an artificial neural network. *Neural Comput. Appl.* **1997**, *5*, 238–247.
169. Laso Bayas, J.C.; See, L.; Fritz, S.; Sturn, T.; Perger, C.; Dürauer, M.; Karner, M.; Moorthy, I.; Schepaschenko, D.; Domian, D.; et al. Crowdsourcing In-Situ Data on Land Cover and Land Use Using Gamification and Mobile Technology. *Remote Sensing* **2016**, *8*, 905.
170. Tewkesbury, A.P.; Comber, A.J.; Tate, N.J.; Lamb, A.; Fisher, P.F. A critical synthesis of remotely sensed optical image change detection techniques. *Remote Sens. Environ.* **2015**, *160*, 1–14.

171. Stehman, S.V.; Fonte, C.C.; Foody, G.M.; See, L. Using volunteered geographic information (VGI) in design-based statistical inference for area estimation and accuracy assessment of land cover. *Remote Sens. Environ.* **2018**, *212*, 47–59.
172. Thompson, I.D.; Maher, S.C.; Rouillard, D.P.; Fryxell, J.M.; Baker, J.A. Accuracy of forest inventory mapping: Some implications for boreal forest management. *For. Ecol. Manage.* **2007**, *252*, 208–221.
173. Bland, M.J.; Altman, D.G. Statistics notes: Measurement error. *BMJ* **1996**, *312*, 1654.
174. Martin, D. An Introduction to "The Guide to the Expression of Uncertainty in Measurement." In *Evaluation of measurement data -- Guide to the expression of uncertainty in measurement*; JCGM, 2008; pp. 1–10.
175. Thanh Noi, P.; Kappas, M. Comparison of Random Forest, k-Nearest Neighbor, and Support Vector Machine Classifiers for Land Cover Classification Using Sentinel-2 Imagery. *Sensors* **2017**, *18*.
176. Song, K. Tackling Uncertainties and Errors in the Satellite Monitoring of Forest Cover Change. **2010**.
177. Foody, G.M. The impact of imperfect ground reference data on the accuracy of land cover change estimation. *Int. J. Remote Sens.* **2009**, *30*, 3275–3281.
178. Foody, G.M. Ground reference data error and the mis-estimation of the area of land cover change as a function of its abundance. *Remote Sens. Lett.* **2013**, *4*, 783–792.
179. Multi-Resolution Land Characteristics Consortium (U.S.) National land cover dataset (NLCD).
180. Menon, S.; Akbari, H.; Mahanama, S.; Sednev, I.; Levinson, R. Radiative forcing and temperature response to changes in urban albedos and associated CO2 offsets. *Environ. Res. Lett.* **2010**, *5*, 014005.
181. Hutyra, L.R.; Yoon, B.; Hepinstall-Cymerman, J.; Alberti, M. Carbon consequences of land cover change and expansion of urban lands: A case study in the Seattle metropolitan region. *Landsc. Urban Plan.* **2011**, *103*, 83–93.
182. Reinmann, A.B.; Hutyra, L.R.; Trlica, A.; Olofsson, P. Assessing the global warming potential of human settlement expansion in a mesic temperate landscape from 2005 to 2050. *Sci. Total Environ.* **2016**, *545-546*, 512–524.
183. Hardiman, B.S.; Wang, J.A.; Hutyra, L.R.; Gately, C.K.; Getson, J.M.; Friedl, M.A. Accounting for urban biogenic fluxes in regional carbon budgets. *Sci. Total Environ.* **2017**, *592*, 366–372.
184. Seto, K.C.; Güneralp, B.; Hutyra, L.R. Global forecasts of urban expansion to 2030 and direct impacts on biodiversity and carbon pools. *Proc. Natl. Acad. Sci. U. S. A.* **2012**, *109*, 16083–16088.
185. Angel, S.; Parent, J.; Civco, D.L.; Blei, A.; Potere, D. The dimensions of global urban expansion: Estimates and projections for all countries, 2000–2050. *Prog. Plann.* **2011**, *75*, 53–107.
186. Coulston, J.W.; Moisen, G.G.; Wilson, B.T.; Finco, M.V.; Cohen, W.B.; Brewer, C.K. Modeling percent tree canopy cover: a pilot study. *Photogrammetric Engineering & Remote Sensing 78 (7): 715--727* **2012**, *78*, 715–727.
187. Reinmann, A.B.; Hutyra, L.R. Edge effects enhance carbon uptake and its vulnerability to climate change in temperate broadleaf forests. *Proc. Natl. Acad. Sci. U. S. A.* **2017**, *114*, 107–112.
188. Rolnick, D.; Veit, A.; Belongie, S.; Shavit, N. Deep Learning is Robust to Massive Label Noise. *arXiv [cs.LG]* 2017.
189. Nachmany, Y.; Alemohammad, H. Detecting Roads from Satellite Imagery in the Developing World. In Proceedings of the Proceedings of the IEEE Conference on Computer Vision and Pattern Recognition Workshops; openaccess.thecvf.com, 2019; pp. 83–89.
190. The SpaceNet Catalog SpaceNet on Amazon Web Services (AWS). "Datasets." 2018.
191. Alemohammad, S.H.; Fang, B.; Konings, A.G.; Aires, F.; Green, J.K.; Kolassa, J.; Miralles, D.; Prigent, C.; Gentine, P. Water, Energy, and Carbon with Artificial Neural Networks (WECANN): A statistically-based estimate of global surface turbulent fluxes and gross primary productivity using solar-induced fluorescence. *Biogeosciences* **2017**, *14*, 4101–4124.
192. McColl, K.A.; Vogelzang, J.; Konings, A.G.; Entekhabi, D.; Piles, M.; Stoffelen, A.

Extended triple collocation: Estimating errors and correlation coefficients with respect to an unknown target. *Geophys. Res. Lett.* **2014**, *41*, 6229–6236.
193. Lyndon D. Estes, Su Ye, Lei Song, Ron Eastman, Sitian Xiong, Tammy Woodard, Boka Luo, Dennis McRitchie, Ryan Avery, Kelly Caylor, Stephanie, Debats. Improving cropland maps through tight integration of human and machine intelligence. *In preparation*.
194. Debats, S.R.; Luo, D.; Estes, L.D.; Fuchs, T.J.; Caylor, K.K. A Generalized Computer Vision Approach to Mapping Crop Fields in Heterogeneous Agricultural Landscapes. *Remote Sens. Environ.* **2016**, *179*, 210–221.
195. Jain, M.; Balwinder-Singh; Rao, P.; Srivastava, A.K.; Poonia, S.; Blesh, J.; Azzari, G.; McDonald, A.J.; Lobell, D.B. The impact of agricultural interventions can be doubled by using satellite data. *Nature Sustainability* **2019**, *2*, 931–934.
196. Pontius, R.G. Criteria to Confirm Models that Simulate Deforestation and Carbon Disturbance. *Land* **2018**, *7*, 105.
197. Schennach, S.M. Recent Advances in the Measurement Error Literature. *Annu. Rev. Econom.* **2016**, *8*, 341–377.
198. Waldner, F.; De Abelleyra, D.; Verón, S.R.; Zhang, M.; Wu, B.; Plotnikov, D.; Bartalev, S.; Lavreniuk, M.; Skakun, S.; Kussul, N.; et al. Towards a set of agrosystem-specific cropland mapping methods to address the global cropland diversity. *Int. J. Remote Sens.* **2016**, *37*, 3196–3231.
199. Castelluccio, M.; Poggi, G.; Sansone, C.; Verdoliva, L. Land Use Classification in Remote Sensing Images by Convolutional Neural Networks. *arXiv [cs.CV]* 2015.
200. Azevedo, T., Sr.; Souza, C.M., Jr.; Shimbo, J.; Alencar, A. MapBiomas initiative: Mapping annual land cover and land use changes in Brazil from 1985 to 2017.; adsabs.harvard.edu, 2018; Vol. 2018.
201. Brown, J.F.; Tollerud, H.J.; Barber, C.P.; Zhou, Q.; Dwyer, J.L.; Vogelmann, J.E.; Loveland, T.R.; Woodcock, C.E.; Stehman, S.V.; Zhu, Z.; et al. Lessons learned implementing an operational continuous United States national land change monitoring capability: The Land Change Monitoring, Assessment, and Projection (LCMAP) approach. *Remote Sens. Environ.* **2019**, 111356.
202. Estes, L.; Elsen, P.R.; Treuer, T.; Ahmed, L.; Caylor, K.; Chang, J.; Choi, J.J.; Ellis, E.C. The spatial and temporal domains of modern ecology. *Nat Ecol Evol* **2018**, *2*, 819–826.
203. Jensen, J.R.; Cowen, D.C. Remote sensing of urban/suburban infrastructure and socio-economic attributes. *Photogramm. Eng. Remote Sens.* **1999**, *65*, 611–622.
204. Dorais, A.; Cardille, J. Strategies for Incorporating High-Resolution Google Earth Databases to Guide and Validate Classifications: Understanding Deforestation in Borneo. *Remote Sensing* **2011**, *3*, 1157–1176.
205. Sexton, J.O.; Urban, D.L.; Donohue, M.J.; Song, C. Long-term land cover dynamics by multi-temporal classification across the Landsat-5 record. *Remote Sens. Environ.* **2013**, *128*, 246–258.
206. Reis, M.S.; Escada, M.I.S.; Dutra, L.V.; Sant'Anna, S.J.S.; Vogt, N.D. Towards a Reproducible LULC Hierarchical Class Legend for Use in the Southwest of Pará State, Brazil: A Comparison with Remote Sensing Data-Driven Hierarchies. *Land* **2018**, *7*, 65.
207. Anderson, J.R. *A Land Use and Land Cover Classification System for Use with Remote Sensor Data*; U.S. Government Printing Office, 1976;.
208. Herold, M.; Woodcock, C.E.; Antonio di Gregorio; Mayaux, P.; Belward, A.S.; Latham, J.; Schmullius, C.C. A joint initiative for harmonization and validation of land cover datasets. *IEEE Trans. Geosci. Remote Sens.* **2006**, *44*, 1719–1727.
209. Carletto, C.; Gourlay, S.; Winters, P. From Guesstimates to GPStimates: Land Area Measurement and Implications for Agricultural Analysis. *J. Afr. Econ.* **2015**, *24*, 593–628.
210. See, L.; Comber, A.; Salk, C.; Fritz, S.; van der Velde, M.; Perger, C.; Schill, C.; McCallum, I.; Kraxner, F.; Obersteiner, M. Comparing the quality of crowdsourced data contributed by expert and non-experts. *PLoS One* **2013**, *8*, e69958.
211. Phinn, S.R. A framework for selecting appropriate remotely sensed data dimensions for environmental monitoring and management. *Int. J. Remote Sens.* **1998**, *19*, 3457–3463.
212. Phinn, S.R.; Menges, C.; Hill, G.J.E.; Stanford, M. Optimizing Remotely Sensed Solutions for Monitoring, Modeling, and Managing Coastal Environments. *Remote Sens. Environ.* **2000**,

*73*, 117–132.
213. Lu, D.; Weng, Q. A survey of image classification methods and techniques for improving classification performance. *International Journal of Remote Sensing* **2007**, *28*, 823–870.
214. Cingolani, A.M.; Renison, D.; Zak, M.R.; Cabido, M.R. Mapping vegetation in a heterogeneous mountain rangeland using landsat data: an alternative method to define and classify land-cover units. *Remote Sens. Environ.* **2004**, *92*, 84–97.
215. Burke, M.; Lobell, D.B. Satellite-based assessment of yield variation and its determinants in smallholder African systems. *Proc. Natl. Acad. Sci. U. S. A.* **2017**.
216. Jin, Z.; Azzari, G.; You, C.; Di Tommaso, S.; Aston, S.; Burke, M.; Lobell, D.B. Smallholder maize area and yield mapping at national scales with Google Earth Engine. *Remote Sens. Environ.* **2019**, *228*, 115–128.
217. Lobell, D.B.; Thau, D.; Seifert, C.; Engle, E.; Little, B. A Scalable Satellite-Based Crop Yield Mapper. *Remote Sens. Environ.* **2015**, *164*, 324–333.
218. Grassini, P.; van Bussel, L.G.J.; Van Wart, J.; Wolf, J.; Claessens, L.; Yang, H.; Boogaard, H.; de Groot, H.; van Ittersum, M.K.; Cassman, K.G. How Good Is Good Enough? Data Requirements for Reliable Crop Yield Simulations and Yield-Gap Analysis. *Field Crops Res.* **2015**, *177*, 49–63.
219. Russakovsky, O.; Deng, J.; Su, H.; Krause, J.; Satheesh, S.; Ma, S.; Huang, Z.; Karpathy, A.; Khosla, A.; Bernstein, M.; et al. ImageNet Large Scale Visual Recognition Challenge. *Int. J. Comput. Vis.* **2015**, *115*, 211–252.
220. Fu, X.; McCane, B.; Mills, S.; Albert, M. NOKMeans: Non-Orthogonal K-means Hashing. In *Computer Vision -- ACCV 2014*; Cremers, D., Reid, I., Saito, H., Yang, M.-H., Eds.; Lecture Notes in Computer Science; Springer International Publishing: Cham, 2015; Vol. 9003, pp. 162–177 ISBN 9783319168647.
221. Basu, S.; Ganguly, S.; Mukhopadhyay, S.; DiBiano, R.; Karki, M.; Nemani, R. DeepSat: A Learning Framework for Satellite Imagery. In Proceedings of the Proceedings of the 23rd SIGSPATIAL International Conference on Advances in Geographic Information Systems; ACM: New York, NY, USA, 2015; pp. 37:1–37:10.
222. Yang, Y.; Newsam, S. Bag-of-visual-words and spatial extensions for land-use classification. *Proceedings of the 18th SIGSPATIAL international* **2010**.
223. Shen, C. A Transdisciplinary Review of Deep Learning Research and Its Relevance for Water Resources Scientists. *Water Resour. Res.* **2018**, *54*, 8558–8593.
224. Stehman, S.V.; Czaplewski, R.L. Design and Analysis for Thematic Map Accuracy Assessment: Fundamental Principles. *Remote Sens. Environ.* **1998**, *64*, 331–344.
225. Stehman, S.V. Practical Implications of Design-Based Sampling Inference for Thematic Map Accuracy Assessment. *Remote Sens. Environ.* **2000**, *72*, 35–45.
226. Aldwaik, S.Z.; Pontius, R.G., Jr. Intensity analysis to unify measurements of size and stationarity of land changes by interval, category, and transition. *Landsc. Urban Plan.* **2012**, *106*, 103–114.
227. Pontius, R.G.; Gao, Y.; Giner, N.M.; Kohyama, T.; Osaki, M.; Hirose, K. Design and Interpretation of Intensity Analysis Illustrated by Land Change in Central Kalimantan, Indonesia. *Land* **2013**, *2*, 351–369.
228. Foody, G.M. Harshness in image classification accuracy assessment. *Int. J. Remote Sens.* **2008**, *29*, 3137–3158.
229. Cohen, J. A Coefficient of Agreement for Nominal Scales. *Educ. Psychol. Meas.* **1960**, *20*, 37–46.
230. Zhang, Q.-M.; Shang, M.-S.; Zeng, W.; Chen, Y.; Lü, L. Empirical comparison of local structural similarity indices for collaborative-filtering-based recommender systems. *Phys. Procedia* **2010**, *3*, 1887–1896.
231. Marçal, A.R.S.; Rodrigues, A.S. A method for multi-spectral image segmentation evaluation based on synthetic images. *Comput. Geosci.* **2009**, *35*, 1574–1581.
232. Rahman, M.A.; Wang, Y. Optimizing Intersection-Over-Union in Deep Neural Networks for Image Segmentation. In Proceedings of the Advances in Visual Computing; Springer International Publishing, 2016; pp. 234–244.
233. Shi, R.; Ngan, K.N.; Li, S. Jaccard index compensation for object segmentation evaluation. In Proceedings of the 2014 IEEE International Conference on Image Processing (ICIP); 2014;

pp. 4457–4461.



**Supplementary Materials**

*Map Accuracy Reporting Practices*

To understand how TD errors can impact map accuracy, it is necessary to first review current practices and standards for measuring and reporting final map accuracy, which are well established in the EO literature[36,37,42,54,75]. While the emphasis of this paper is specifically on TD, as opposed to map reference data, it is necessary to review procedures for accuracy assessment. Sampling protocols for accuracy assessment are more stringent than those for the collection of TD[54], but because both training and map reference data are often collected as part of a single campaign or using the same methods[e.g. 52], the stricter set of procedures should be followed for both. We therefore summarize several important features and best practices for error analysis.

Error analysis compares a mapped variable to a corresponding map reference variable. Map reference data used for accuracy assessment are collected according to sampling and response designs that specify, respectively, the probabilities of inclusion for each location, and the protocol for creating the labeled map reference data[54,224]. Map reference data and TD may both be collected as part of a single larger sample[8], provided there is strict separation between the two datasets. Sampling design, whether simple random, stratified random, or systematic is dependent on application and *a priori* knowledge of the study area, and should be probability-based, such that the inclusion probability of each sample relates to the likelihood of that sample unit being included[36,54,225]. If the observations do not have equal probability of selection, then it is essential to convert the sample data to a confusion matrix (i.e. a square contingency table) that reflects an unbiased estimate for the entire population using methods summarized in Stehman and Foody[54].

Map accuracy is typically assessed using a metric or metrics designed to provide information regarding the correspondence of mapped and reference data. The objective of these metrics is to provide insights into the product's expected best use cases and potential shortcomings. Accuracy metrics vary according to whether the mapped variable is categorical or continuous, with each type of variable having its own foundation for error analysis[79–83]. The confusion matrix is the foundation for categorical variables. Conventionally, the table's rows provide mapped categories and the columns show the matching reference categories, with the diagonal entries showing agreement between the two. The confusion matrix is used to calculate user's accuracy (i.e. the complement of commission error), producer's accuracy (i.e. the complement of omission error), and overall accuracy (i.e. the complement of proportion error)[38]. More details on the interpretation of these values and other aspects of the error matrix are provided in several existing publications[34,36,54,79,226–228].

Several other accuracy measures are also calculated from the error matrix. Most prominent among these is the Kappa Index of Agreement[229], which is widely used in the remote sensing and species distribution modelling literature. However, Kappa varies with class prevalence[84] and can be easily misinterpreted, thus its use is no longer recommended[37]. More recently, a number of additional metrics have started to be more commonly used in EO accuracy analysis, in part due to contributions from other disciplines, such as computer science. Due to differing conventions and objectives within these disciplines, the metrics and terminology relating to error and accuracy are

[8] It is often advantageous to have a separate train sample design, however, as these may be more purposive and targeted to classes of interest[54].

often quite different. To help resolve this confusion, we summarize these metrics and their meanings in Table S1.

A special and increasingly used type of categorical map is derived from Object-Based Image Analysis (OBIA), in which the output map is classified into polygons representing discrete objects[90]. At present there is no commonly accepted standard for reporting the accuracy of such maps in the remote sensing literature[62], since the optimal set of metrics for polygon accuracy assessment depends on the intended use of the categorical map. For example, edge similarity metrics are useful for assessing the segmentation of individual agricultural fields, whereas area based metrics will fail where multiple objects are frequently mapped as a single object[62]. The Jaccard Index, also called Intersection over Union, is a commonly used benchmark in the computer vision and segmentation literature for evaluating polygon-to-polygon classification accuracies, and has the advantage of being straightforward to calculate and interpret[e.g 230,231–233]. This and other similar area-based metrics can be used in a remote sensing context, and thus may help to strengthen communication between EO and computer vision researchers. However, we caution that for many mapping goals, these metrics should be complemented by others that account for shape and edge similarity. Perhaps due to these complexities, many existing studies have assessed the accuracy of object-based maps using per-pixel accuracy assessments, which itself is problematic because it involves comparing fundamentally different spatial units[62].

The scatter plot, showing the mapped variable on the y-axis and the reference variable on the x-axis, is the foundation of error analysis for continuous variables. Since any point falling off the 1:1 line indicates deviation from a measurement of the true value, a visual assessment of the plot is an intuitive first step for assessing error in the mapped variable. Several metrics are commonly used to quantify disagreement between mapped and reference variables, including mean deviation, Root Mean Square Error (RMSE; a.k.a. Root Mean Square Deviation, RMSD), and Mean Absolute Deviation (MAD). The use of RMSE may be inappropriate, since it combines MAD with the variation among the deviations, and is frequently misinterpreted as the measurement of average error[85–87]. The Receiver Operating Characteristic (ROC) and the Total Operating Characteristic (TOC) enable analysis of a continuous mapped variable relative to a binary reference variable, for example presence or absence[81,88,89]. The area under this curve (AUC) of an ROC/TOC plot is often used as a single measure of overall accuracy that summarizes numerous thresholds for the continuous variable[89].

Most of the metrics reported above (Table 1) provide useful information for users about map reliability. However, the usefulness of that information depends on the map reference data having higher accuracy than the mapped data, which is an assumption that is often unexamined[31,178]. This tendency is illustrated by Ye et al.[62], who reviewed 209 journal articles focused on object-based image analysis and found that one third gave incomplete information about the sample design and size of their map reference data, let alone any mention of error within the sample. Errors in map reference data can bias the map accuracy assessment[44,149], as well as estimates derived from the confusion matrix, such as land cover class proportions and their standard errors[43]. To correct for such biases caused by map reference error, one can use published procedures for estimating map reference data accuracy[44] and to calculate variance measures for area estimates[43]. These approaches depend on quantifying errors in the map reference data. For the common case of image-interpreted map reference data, this can be achieved by having multiple interpreters create reference polygons and labels for the same locations, and then calculating the level of agreement in their categorical labels[31,54,149,153]. Additionally, knowledge of this uncertainty can be quantitatively incorporated into continuous estimates based on the image interpreted data[43]. *In situ* observations can similarly be used to assess the accuracy of image-interpreted map reference samples[57], although their availability is often limited by cost considerations.

1792 Table S1: Summary of commonly used error metrics.

| Term | Information Content/Typical Usage | Description |
|---|---|---|
| Overall Accuracy | Summary metric combining all class accuracies into a single number | Proportion of correctly classified cases divided by the total of all classified cases |
| User's Accuracy (a.k.a. Precision) | Metric of the intensity of true positives given the classified category in which the true positives were 'found'. The intensity complement of commission error. | Proportion of correctly classified cases relative to the total number of cases classified into the given category |
| Kappa Index of Agreement | Single metric for overall accuracy | Used to measure the agreement between mapped and reference categories of a dataset while attempting to correct for agreement that occurs by chance. |
| Producer's Accuracy (a.k.a. Sensitivity, Recall) | Metric indicating the intensity of true positives given the reference category) The intensity complement of omission error. | True positive rate; ratio of correctly classified cases of a given class to the total true cases of that class |
| Specificity | Metric for commission error; indicates how well the model avoids false positives | True negative rate; ratio of correctly classified negatives to the sum of true negatives and false positives |
| True Skill Statistic [78] | Metric that combines sensitivity and specificity while accounting for class prevalence | Sensitivity + Specificity - 1 |
| F1 [79,80] | Combined metric of commission and omission error | Equally weighted harmonic mean of precision and recall |
| Bias (Mean Bias Error) | Quantifies the average difference between predicted and reference variables | The average error, representing the systematic over- or under-prediction of a continuous variable |
| Root Mean Square Error/Deviation | Measures a combination of the average error and the variability within the distribution of errors | A potentially misleading metric used to measure disagreement between predicted and reference continuous variables |
| Mean Absolute Deviation | Measures how far points are from Y=X line | Recommended metric to measure disagreement between predicted and reference continuous variables |
| Jaccard Index, also called Intersection over Union | Between two discrete/crisp datasets, reports the area of intersection divided by the area of union. | Most commonly used metric to indicate accuracy of object-based classification, which is also called semantic segmentation. |

1793

1794

*Triple Collocation RMSE*

TC-based RMSE estimates at each pixel were used to compute *a priori* probability ($P_i$) of selecting a particular dataset:

$$P_i = \frac{\frac{1}{\sigma_{\varepsilon_i}^2}}{\sum_{i=1}^{3} \frac{1}{\sigma_{\varepsilon_i}^2}} \qquad \text{(eq. S1)}$$

$P_i$ is the probability of selecting measurement system i, $\sigma_{\varepsilon i}$ is the standard deviation of the random error in measurement system i.

Figure S1 depicts how $X_T$ (the training time series for a pixel) is formed by sampling from $X_1$, $X_2$, and $X_3$ over time.

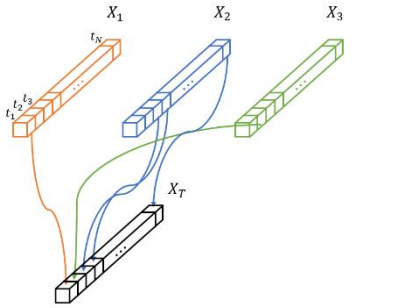


Figure S1: Schematic of product selection using the Triple Collocation approach.

Table S2: Quantitative results of comparing each of the three models trained for the road detection case in Kumasi, Ghana to the validation labels. This region (shown in Figure 9) included 5,406,942 road pixels and 50,627,010 background pixels.

| | **F1** | **IOU** | **Precision** | **Recall** |
|---|---|---|---|---|
| Khartoum Model | | | | |
| Average | 0.6659 | 0.5723 | 0.7758 | 0.6267 |
| Road | 0.3780 | 0.2330 | 0.6250 | 0.2709 |
| Background | 0.9538 | 0.9116 | 0.9266 | 0.9862 |
| Kumasi Model | | | | |
| Average | 0.8004 | 0.6955 | 0.7693 | 0.8450 |
| Road | 0.6458 | 0.4769 | 0.5662 | 0.7513 |
| Background | 0.9552 | 0.9142 | 0.9725 | 0.9386 |
| Khartoum Model retrained in Kumasi | | | | |
| Average | 0.7869 | 0.6830 | 0.7965 | 0.7780 |
| Road | 0.6135 | 0.4425 | 0.6363 | 0.5921 |
| Background | 0.9603 | 0.9236 | 0.9568 | 0.9639 |

Table S3: Template and procedure for documenting training data. Note that the 'values' column is intentionally left blank, as this is merely an example. We would expect a fully filled out table to be several pages in length due to the technical nature of the metadata explanation.

| **Metadata Category** | **Value** |
|---|---|
| Training data set name | |
| How data were created (technical details, to include number of analysts, whether *in situ* or image interpretation, samples of field sheets, copies of materials used to educate analysts, date of data creation, etc.) | |
| Funding source | |
| Purpose | |
| LULC definitions | |
| Time period | |
| Spatial extent | |
| Spatial resolution (image, field, quadrat, point location) | |
| Image ID (sensor specific unique identification information) | |

(a) (b)


Figure S2: Sample prediction results in Kumasi, Ghana. (a) Input imagery. (b) Predictions from the Las Vegas model. (c) Predictions from the Khartoum model. (d) Prediction from the Kumasi model. (e) Predictions from the Khartoum Model retrained in Kumasi. [In panel b-e model predictions are in shaded color overlaid with validation labels in red on top of imagery.]

Figure S2 shows a qualitative comparison of different model outputs along with the validation labels over a sample area of Figure 4.